Compositional and Structural Analysis of a $(PhSiO_{3/2})_{0.35}(MeSiO_{3/2})_{0.40}(Me_2ViSiO_{1/2})_{0.25}$ Resin

Duane R. Bujalski,[†] Huiping Chen,[‡] Ronald E. Tecklenburg,[‡] Eric S. Moyer,[§] Gregg A. Zank,[†] and Kai Su*,[†]

New Venture Business, Analytical Sciences, and Microelectronics, Dow Corning Corporation, Midland, Michigan 48686-0995

Received September 6, 2002

ABSTRACT: Silsesquioxanes have been postulated to have complex structures due to varieties of siloxane bond arrangements from intra- or intermolecular condensation reactions. However, most structure types reported in the literature such as ladder or cage structures were proposed on the basis of spectroscopic analysis of the crude product and therefore may have overlooked the structural complexity of these resinous materials. In this study, a $(PhSiO_{3/2})_{0.35}(MeSiO_{3/2})_{0.40}(Me_2ViSiO_{1/2})_{0.25}$ ($T^{Ph}_{0.35}T^{Me}_{0.40}M^{Vi}_{0.25}$) silsesquioxane was fractionated into 13 fractions by supercritical fluid extraction and analyzed by mass spectrometry (MS), nuclear magnetic resonance (NMR), Fourier transform infrared spectroscopy (FTIR), and size exclusion chromatography (SEC) techniques. Detailed compositional, structural, and molecular weight information on the parent silsesquioxane and individual fractions were obtained. The average composition obtained by NMR varied for the individual fractions, where the $Me_2ViSiO_{1/2}$ content was higher in the low-molecular-weight fractions but remained relatively constant for the high-molecular-weight fractions. On the basis of gas chromatography−mass spectrometry (GC-MS) and electrospray ionization Fourier transform mass spectrometry (ESI FTMS) results for the six lowest molar mass fractions 1−6, the individual species that were identified can be summarized into three general categories: (1) T_nM_{n+2}, (2) $T_{2n+1}M_{2m+1}$ (odd number of T and M), and (3) $T_{2n}M_{2m}$ (even number of T and M). Species with the T_nM_{n+2} composition have linear or hyperbranched structures while one or more siloxane rings are required for the $T_{2n}M_{2m}$ and $T_{2n+1}M_{2m+1}$ compositions. Combining ^{29}Si NMR and FTIR results, we propose that individual molecules in the silsesquioxane adopt structures composed of predominantly fused siloxane rings connected via adjacent (ladderlike) or nonadjacent vertexes (cagelike). Conformational analysis through SEC yielded a Mark−Houwink "*a*" parameter of 0.64−0.72 in THF for the fractions with M_w between 1750 and 26 900 g/mol, which was consistent with a random coil conformation. The flexible nature of the silsesquioxane molecules appeared to confirm the proposed "linear" fused ring structure. Light scattering results for fraction 13 (M_w 60 800) and its slightly lower "*a*" value of 0.502 suggest a higher degree of branching for the structures present in the highest molecular weight fraction.

Introduction

Silsesquioxane can be viewed as organic−inorganic hybrids that combine many desirable properties of conventional organic and inorganic components, such as good photostability, thermal stability and chemical resistance.[1−3] Compared to inorganic glasses, silsesquioxanes exhibit improved processability, i.e., solubility or flowability, at relatively low temperatures, which allows for the formation of materials in complicated geometries or shapes including films, coatings, and fibers. There is currently considerable interest in developing specialty silsesquioxanes that can be used as precursors to ceramic materials,[4−10] low dielectric constant (*k*) interlayer dielectric materials,[11−19] and photonic materials for waveguides and devices that exploit the large thermooptical effect of siloxanes.[20−23] An additional advantage of siloxane materials over organic materials is that many of the unique electric, optical, and mechanical properties can be efficiently tuned through material design.

Silsesquioxanes are generally prepared by hydrolysis and condensation of chlorosilane or alkoxysilane with a general formula $RSiX_3$, where X is either Cl or an alkoxy group and the organic group R can be modified to achieve desired material properties. Since a variety of structures such as linear, ladder, and cages are possible due to intra- or intermolecular condensation, it is now generally accepted that these materials adopt more complicated three-dimensional structures than the ladder structure originally proposed by Brown.[24,25] The nature of the monomer, such as the bulkiness of the organic group on silicon, the polarity of reaction medium, the presence of templating reagents,[26,27] and the type of catalyst, could all greatly impact the structure or the distribution of species with varying structural features. For example, polyhedral cages can be obtained by careful selection of reaction conditions.[28−30] A silsesquioxane could potentially have one or several predominant structural types or a combination of these types for a given composition, and most likely the main structural types along with molecular weight distribution will have the greatest influence on material properties. A more thorough understanding of the correlation between the physical properties and structural features will further help the optimization of the material design through synthesis.

In a separate paper, we reported the synthesis of a $T^{Ph}_{0.35}T^{Me}_{0.40}M^{Vi}_{0.25}$ silsesquioxane and demonstrated the dependence of molecular weight distribution upon reaction conditions.[31] In this study, the resin was fractionated into 13 fractions by supercritical fluid

* Corresponding author. E-mail k.su@dowcorning.com.
† New Venture Business.
‡ Analytical Sciences.
§ Microelectronics.

10.1021/ma025652h CCC: $25.00
Published on Web 12/14/2002

extraction (SFE). Individual fractions were analyzed by MS, NMR, FTIR, and SEC, yielding detailed compositional, structural, and molecular weight information. GC-MS and ESI FTMS were used to deduce the composition of individual species present in each fraction while FTIR and NMR provided the average structural information. The molecular mass distributions obtained by MALDI−TOF MS were compared with values obtained by SEC using a column calibrated with polystyrene standards or a setup of right-angle laser light scattering (RALLS), viscometry, and refractive index (RI) triple detection. On the basis of available analytical data, we propose the $T^{Ph}_{0.35}T^{Me}_{0.40}M^{Vi}_{0.25}$ resin adopts structures containing predominantly fused siloxane rings connected via adjacent (ladderlike) or nonadjacent vertices (cagelike).

Experimental Section

Materials. All organosiloxane materials were obtained from Dow Corning Corp. as intermediates or purchased from Hüls America. Trifluoromethanesulfonic acid was obtained from Aldrich. Toluene, KOH, and calcium carbonate were purchased from Fisher. 3% aqueous KOH was prepared before use.

Analytical Techniques. *Nuclear Magnetic Resonance.* Solution NMR spectra were recorded on a Varian VXR400S with $CDCl_3$ in a 5 mm switchable probe or a 16 mm Si-free probe. $Cr(acac)_3$ was added to the solution prior to ^{29}Si measurements to ensure quantitative acquisition.

Fourier Transform Infrared Spectroscopy. FTIR spectra were collected on a Perkin-Elmer 1600 Fourier transform infrared spectrometer with KBr salt plate. The silsesquioxane samples were first dissolved in CCl_4 and then dispersed onto a KBr plate. The FTIR spectra were measured from thin films obtained after evaporation of CCl_4 solvent.

Mass Spectrometry. GC-MS analysis was performed on a Hewlett-Packard 5973 series GC-MS instrument equipped with a 105 m long and 0.25 mm internal diameter Rtx1 column. The oven was heated from 30 to 280 °C with a ramp rate of 5 °C/min.

The ESI FTMS data were collected on a Bruker (Billerica, MA) Apex II Fourier transform ion cyclotron resonance (FTICR) mass spectrometer equipped with a 4.7 T superconducting magnet and an external Analytica electrospray ionization (ESI) source (Branford, CT). A Cole-Parmer (Vernon Hills, IL) series 74900 syringe pump was used to continuously infuse samples into the ESI source at a flow rate of 0.3 mL h^{-1}. The external electrospray ion source was operated with a 45° off-axis sprayer. High-purity (99.995%) nitrogen gas was used both as a nebulizing gas at ambient temperature and as a drying gas at 105 °C. An electrostatic potential of ca. −4.7 kV (relative to the grounded needle) was applied to the metal-capped glass capillary. Ions were accumulated in a hexapole ion guide, adjacent to the external ESI source, and were subsequently injected into the INFINITY cell using the patented Sidekick method. Data acquired in the broadband mode were typically collected using 512K data points for fractions 1−3 and using 128K data points for fractions 4−6. The measured *m*/*z* values are the average values of multiple replicate measurements and, in some cases, obtained via internal calibration. This was especially necessary for fractions 4−6 since resolution and mass accuracy decline for higher molecular weight species. About 100 ppm (v/v) solutions of the fractions were prepared in a 1:1 (v/v) mixture of $CHCl_3$ and MeOH with 1 mM NH_4OAc present in the MeOH solution to assist in the ionization of siloxane species. In the positive-ion mode, the ions detected in the ESI FTMS experiment were typically $[M + NH_4]^+$ ions with little or no fragmentation.

MALDI−TOF MS data were collected in the linear mode using a Bruker Biflex III time-of-flight mass spectrometer with delayed ion extraction. The fractions were dissolved in chloroform, as was the matrix, dithranol. AgTFA was also added to the matrix solution. Approximately 0.5 μL of the solution containing matrix and cationization reagent was spotted onto the probe followed by 0.5 μL of the analyte solution. Minimum laser power was used to avoid excessive fragmentation. Each spectrum represents the sum of 1000 scans. The ions detected in the positive-ion mode were typically $[M + Ag]^+$ ions.

Size Exclusion Chromatography. SEC data were obtained on a Waters instrument equipped with two mixed bed Series D PL gel columns, a model 600E systems controller, and a model 410 differential refractometer detector. The SEC columns were calibrated with polystyrene standards using THF as the eluting solvent. SEC using triple detectors was performed on a Waters 2690 Alliance System using two Polymer Laboratories Plgel Mixed-D (300 × 7.5 mm, 5 μm, 200−200 000 Da exclusion limit) styrene−divinylbenzene columns preceded by a Polymer Laboratories Plgel guard column (50 × 7.5 mm, 5 μm). The columns were thermostated at 30 °C. The detection system consisted of a Viscotek T60 multiple detector (viscosity and right angle laser light scattering) and a Viscotek model 125 differential laser refractometer. HPLC grade THF (Fisher Scientific) was used as the eluent. A flow rate of 1 mL/min and a 100 μL injection volume were used. Typical sample concentrations of 1% (w/v) were used.

Elemental Analysis. CHN analysis was performed using a Perkin Elemer 2400 analyzer. Silicon analysis was determined by a fusion technique that involved converting the solid into a soluble form and analyzing the solute for total silicon by Arl 3580 ICP-AES analysis.

Synthesis of $(PhSiO_{3/2})_{0.35}(MeSiO_{3/2})_{0.40}(Me_2ViSiO_{1/2})_{0.25}$. A mixture of phenyltrimethoxysilane (277.6 g, 1.4 mol), methyltrimethoxysilane (218.0 g, 1.6 mol), and 1,1,2,2-tetramethyl-1,2-divinylsiloxane (93.6 g, 0.56 mol) was charged into a 3 L flask equipped with a condenser and a mechanical stirrer under argon. A 6.8 g sample of trifluoromethanesulfonic acid that was dissolved in 20 mL of deionized water was added to the reaction flask upon which the solution immediately turned yellow. After the mixture was heated to reflux temperature for 90 min, 800 mL of toluene and 300 mL of water were added. The solution was then heated to reflux temperature for an additional 90 min. Calcium carbonate (12 g, 0.12 mol) was added, and the solvent was distilled until the overhead temperature increased to ca. 81 °C (605 mL of toluene was collected in the distillate). Additional toluene (365 mL) was added to adjust the nonvolatile siloxane content to 47%. Aqueous 3 wt % potassium hydroxide (40 mL, 0.021 mol) was added, and the water was azeotropically removed using a Dean−Stark apparatus. After the reaction mixture was dried (ca. 4 h), the reflux was continued for 9.5 h before cooling to 50−60 °C. Chlorodimethylvinylsilane (22.1 g, 0.18 mol) was added, and the solution was stirred at room temperature overnight. The solution was first filtered through a Celatom filter-aid, followed by further filtration through a 0.45 μm membrane. The solution was then vacuum-dried to yield a light yellow gum. Anal. Found: C, 43.06%; H, 5.30%; Si, 20.2%. ^1H NMR ($CDCl_3$, 200.1 MHz, ppm): 0.25 (br, CH_3), 3.50 ($SiOCH_3$), 5.84 ($CH{=}CH_2$), 6.09 ($CH{=}CH_2$), 7.10 (C_6H_5), 7.81 (C_6H_5). $^{29}Si\{^1H\}$ NMR ($CDCl_3$, 79.4 MHz, ppm): −2.0 ($Me_2ViSiO_{3/2}$), −57.5 ($Me(ZO)SiO_{2/2}$), −65.8 ($MeSiO_{3/2}$), −70.5 ($Ph(ZO)SiO_{2/2}$), −79.9 ($PhSiO_{3/2}$), −80.5 ($PhSiO_{3/2}$). IR (KBr, cm^{-1}): 3051 w, 2965 w, 1595 w, 1430 w, 1407 w, 1270 m, 1132 vs, 1049 s, 837 m, 785 m, 719 m, 698 m, 484 m.

Supercritical Fluid Extraction. A 450.8 g sample of $(PhSiO_{3/2})_{0.35}(MeSiO_{3/2})_{0.40}(Me_2ViSiO_{1/2})_{0.25}$ silsesquioxane was fractionated into 13 fractions using CO_2 supercritical fluid extraction at Phasex Corp. After fractionation, 425.0 g (94.3%) of the material was recovered. In a control experiment, a small sample was processed using supercritical fluid CO_2 under similar fractionation conditions without separation. The SEC analysis of the silsesquioxane before and after the treatment showed a negligible difference, indicating complete solublility in supercritical fluid CO_2 and stability under fractionation processing conditions. In the following discussion, fraction 1

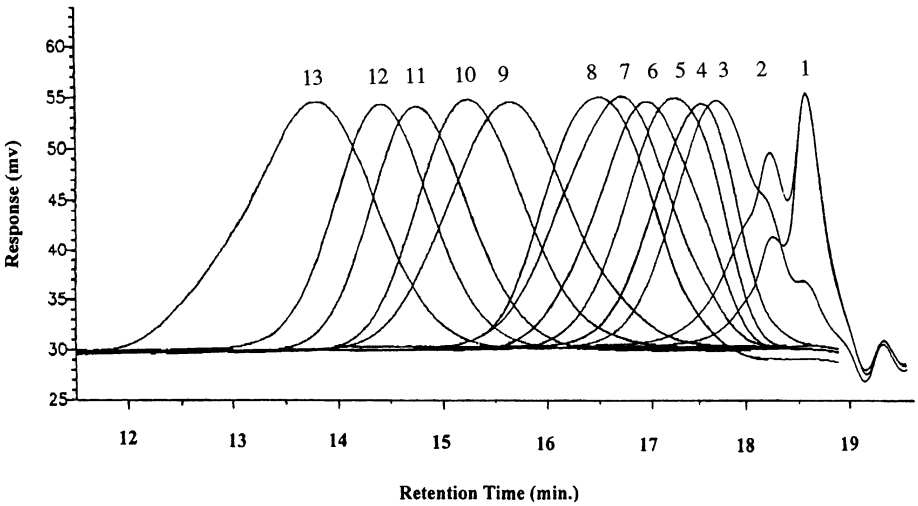

Figure 1. Overlay of GPC chromatograms for resin fractions.

denotes the lowest mass fraction, and the increase in numerical designation coincides with the increase in MW.

Results and Discussion

The $(PhSiO_{3/2})_{0.35}(MeSiO_{3/2})_{0.40}(Me_2ViSiO_{1/2})_{0.25}$ resin was synthesized by hydrolysis and condensation of $MeSi(OMe)_3$, $PhSi(OMe)_3$, and $(Me_2ViSi)_2O$ according to eq 1:

$$x\mathrm{PhSi(OMe)_3} + y\mathrm{MeSi(OMe)_3} + z(\mathrm{Me_2ViSi})_2\mathrm{O} + \mathrm{H_2O}$$
$$\text{(excess)} \xrightarrow{\mathrm{CF_3SO_3H}} \text{cohydrolyzate} \xrightarrow{\text{3\% KOH}} \xrightarrow{\mathrm{Me_2ViSiCl}}$$
$$(PhSiO_{3/2})_{0.35}(MeSiO_{3/2})_{0.40}(Me_2ViSiO_{1/2})_{0.25} \quad (1)$$

The silsesquioxane was isolated as a soft solid with $M_w = 9800$ and $M_n = 2800$ measured initially by SEC calibrated with polystyrene standards. The fractions from SFE were recovered as liquids, oils, gums, or white brittle solids, depending upon their molecular weight. The weight-average molecular weight (M_w) ranged from 490 to 26 200 g/mol whereas polydispersity was relatively narrow ($M_w/M_n < 1.3$). However, the normalized SEC chromatograms shown in Figure 1 indicate polymodal distributions for fractions 1−3. Otherwise, the chromatograms for fractions 4−12 appeared more symmetrical and monodispersed. The SEC chromatogram of the highest molecular weight fraction, fraction 13 skewed toward a lower retention time, or higher molecular weight, implying the presence of molecular/structural components unique to this fraction.

GC-MS, ESI FTMS, and MALDI−TOF MS Analysis. Mass spectrometry has become an extremely valuable tool for the characterization of silsesquioxanes, especially with the application of soft ionization techniques such as electrospray ionization (ESI)[32,33] and matrix-assisted laser desorption/ionization (MALDI).[34−36] Among all existing MS instruments, Fourier transform ion cyclotron resonance mass spectrometry (FTICR-MS, also called FTMS)[37−40] offers ultra high resolution and mass accuracy which are extremely important for the separation and identification isobaric ions for complex silsesquioxane samples.[41] In addition to structural information, molar mass distributions of silsesquioxanes can be conveniently obtained using MALDI−TOF MS. In this study, the six lowest molar mass fractions were characterized using ESI FTMS, whereas five higher molar mass fractions were analyzed using MALDI−TOF MS. In addition, GC-MS was also used to characterize the three lowest molar mass fractions.

GC-MS. For convenience in the following discussion, the $PhSiO_{3/2}$, $MeSiO_{3/2}$, $Me_2ViSiO_{1/2}$, and $MeO_{1/2}$ groups are denoted as T^{Ph}, T^{Me}, M^{Vi}, and M^{OMe}, respectively. Using such notation, $Ph(MeO)Si(OSiMe_2Vi)_2$, for example, can be represented as $T^{Ph}M^{Vi}{}_2M^{OMe}$. In general, the species observed by GC-MS in fractions 1−3 fall into three categories: (1) monomeric and dimeric molecules, $T^{Me}M^{Vi}{}_3$ (MW 346) $T^{Ph}M^{Vi}{}_3$, (MW 408), $T^{Ph}{}_2M^{Vi}{}_4$ (MW 630), $T^{Me}{}_2M^{Vi}{}_4$ (MW 506), and $T^{Me}T^{Ph}M^{Vi}{}_4$ (MW 568); (2) methoxy and silanol containing molecules (MW 276, $T^{Me}M^{Vi}{}_2M^{OMe}$; MW 262, $T^{Me}M^{Vi}{}_2M^{OH}$; MW 420, $M^{Vi}{}_3T^{Me}$; MW 436, $T^{Me}{}_2M^{OMe}M^{Vi}{}_3$; MW 338, $T^{Ph}M^{Vi}{}_2M^{OMe}$; MW 498, $T^{Ph}T^{Me}M^{Vi}{}_3M^{OMe}$; MW 560, $T^{Ph}{}_2M^{Vi}{}_3M^{OMe}$) from incomplete condensation of alkoxysilanes; and (3) $Me_2SiO_{2/2}$ containing molecules most likely derived from impurities in the starting materials. The peak intensities of "dimers" such as $T^{Ph}{}_2M^{Vi}{}_4$, $T^{Me}{}_2M^{Vi}{}_4$, and $T^{Me}T^{Ph}M^{Vi}{}_4$ increased from fraction 1 to 3 while that of monomers like $T^{Me}M^{Vi}{}_3$ and $T^{Ph}M^{Vi}{}_3$ decreased. The number of species at higher retention times increased significantly for fraction 3. Consequently, identification of these compounds by electron-impact (EI) mass spectrometry became more difficult and was, therefore, not attempted.

ESI FTMS. The ESI FTMS spectra for fractions 1−3 are shown in Figure 2. For fractions 1 and 2, the ions observed were mostly below *m/z* 1000, while the spectrum for fraction 3 clearly contained ions above *m/z* 1000. The composition assignments based upon exact mass measurements are listed in Table 1. Ions identified in all three fractions, although differing in abundance, corresponded to the same molecular species. The most abundant ions located at *m/z* 586.21334 ($T^{Me}T^{Ph}M^{Vi}{}_4$) and *m/z* 648.23070 ($T^{Ph}{}_2M^{Vi}{}_4$) were assigned to M_4T_2 dimers. As a comparison, the most intense peaks in the GC-MS chromatograms were due to the monomeric compounds $T^RM^{Vi}{}_3$ (MW 408, $T^{Ph}M^{Vi}{}_3$; MW 346, $T^{Me}M^{Vi}{}_3$).

The ESI FTMS spectra for fractions 4−6 (Figure 3a−c) exhibited significantly different features compared with those for fractions 1−3. The large number of ions observed reflected the complexity of these silsesquioxane fractions due to various combinations of T^{Ph}, T^{Me}, and M^{Vi}. The composition assignments for ions having

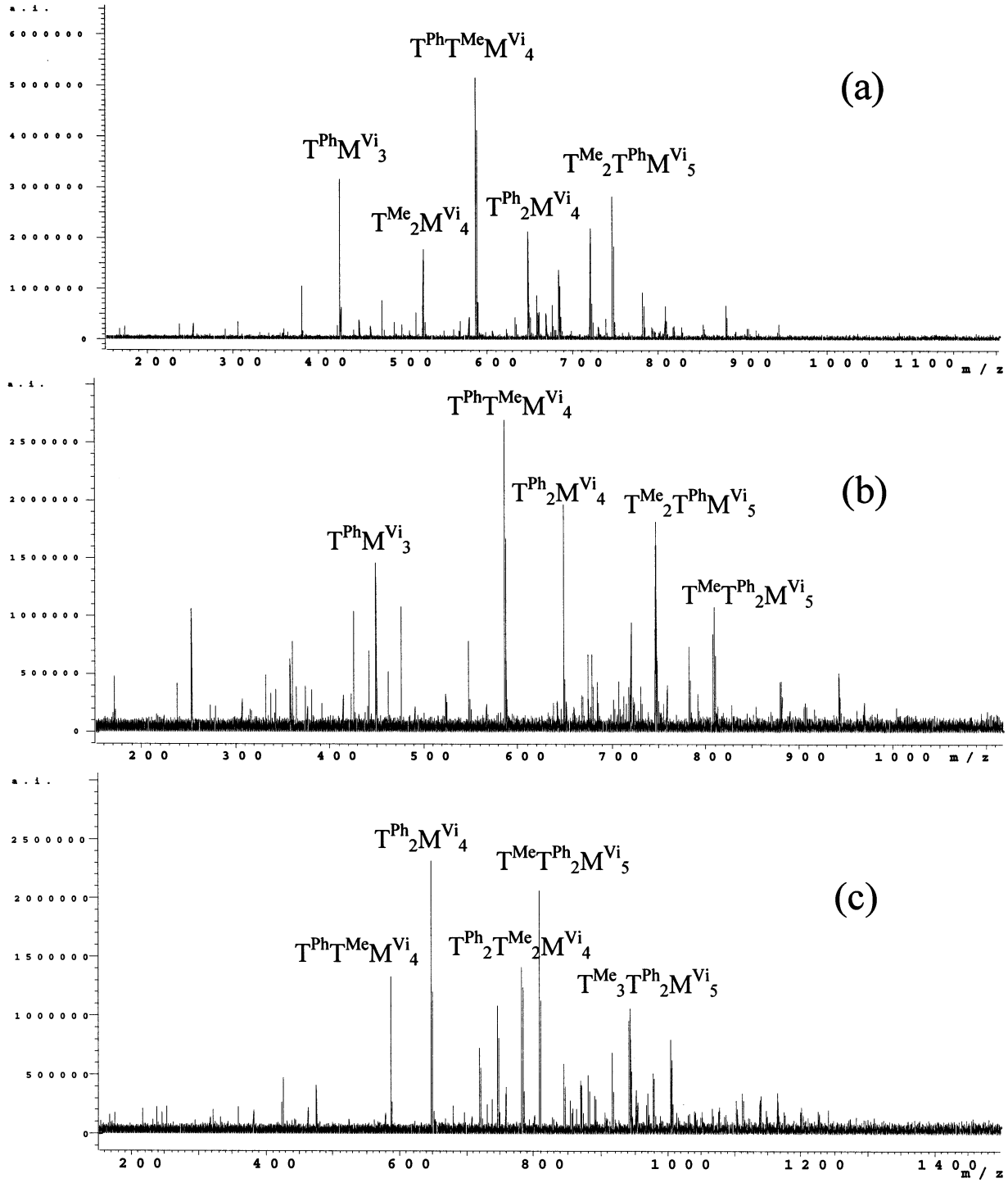

Figure 2. ESI FTMS spectra of (a) fraction 1, (b) fraction 2, and (c) fraction 3.

relative intensities greater than 10% are listed in Table 2. Mass measurement errors between experimental and theoretical values were less than 10 ppm in all cases and less than 5 ppm in most cases. The majority of the species identified contained $Me_2ViSiO_{1/2}$ end groups; however, molecules with methoxy end groups were also observed.

The results shown in Tables 1 and 2 indicated that ions seemed to appear in sets due to different combinations of T^{Ph} and T^{Me}. For example, a T_3M_5 formulation would include four possible combinations, $T^{Ph}{}_3M^{Vi}{}_5$, $T^{Ph}{}_2T^{Me}M^{Vi}{}_5$, $T^{Ph}T^{Me}{}_2M^{Vi}{}_5$, and $T^{Me}{}_3M^{Vi}{}_5$, all of which were observed in the ESI FTMS data. Given T^{Ph} and $T^{Me} = T$, all compositions identified can be reduced to the general formula listed in the seventh column in Tables 1 and 2 to represent different ion "sets". The center ions of each set were abundant due to the most probable combinations of T^{Me} and T^{Ph}. The overall spectra for these fractions can be visualized by superimposing cluster peaks from different "sets". On the basis of the reduced representations of these "sets", the species identified in these fractions can be summarized into three general formulas: (1) T_nM_{n+2}; (2) $T_{2n+1}M_{2m+1}$ (odd number of T and M, e.g., $T_{2n+1}M_3$, $T_{2n+1}M_5$, $T_{2n+1}M_7$, etc.); (3) $T_{2n}M_{2m}$ (even number of T and M, e.g., $T_{2n}M_4$, $T_{2n}M_6$, $T_{2n}M_8$, etc.). Scheme 1 shows the derivation of the general formula for the species observed.

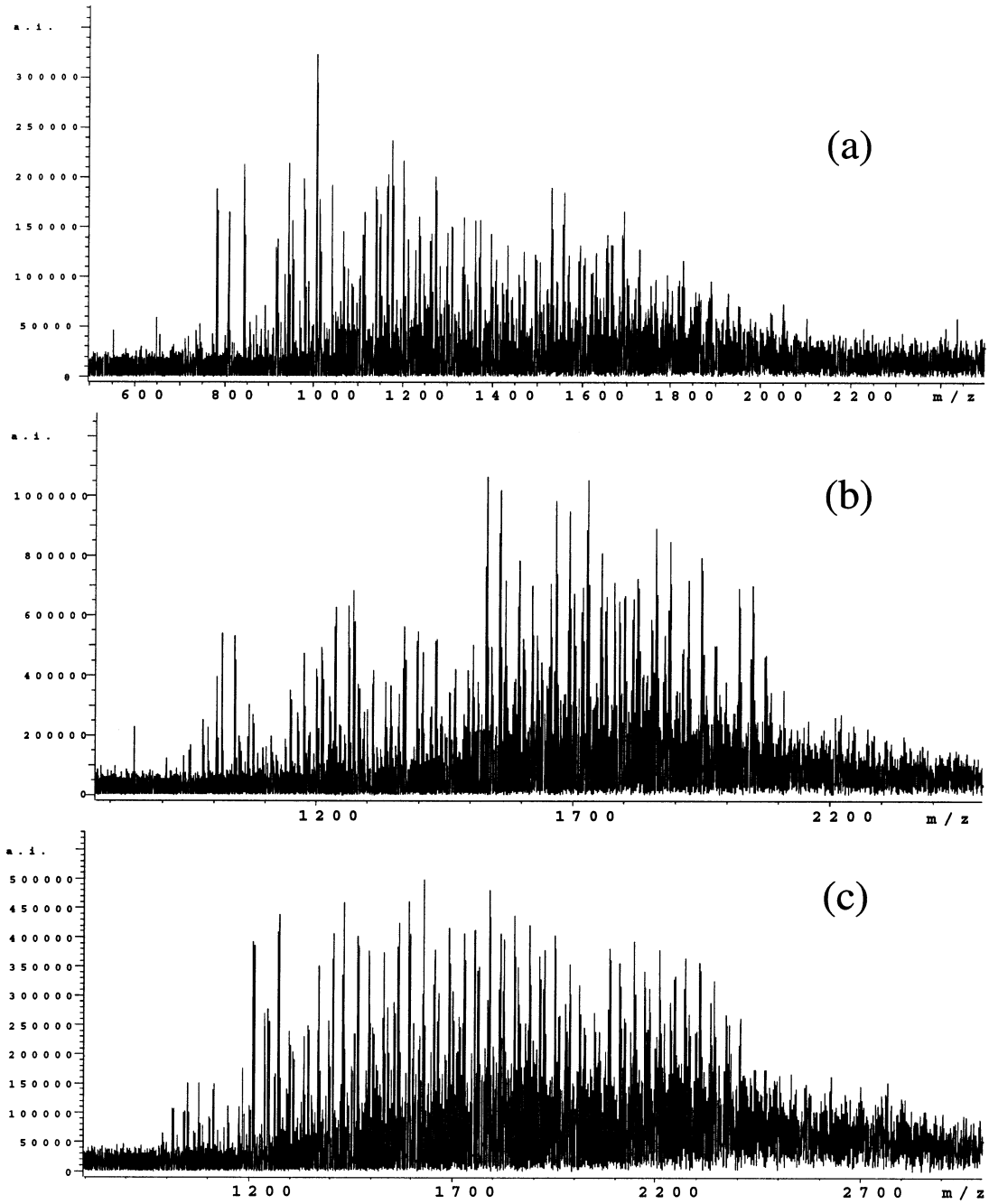

Figure 3. ESI FTMS spectra of (a) fraction 4, (b) fraction 5, and (c) fraction 6.

T_nM_{n+2} represent species having linear or hyperbranched structures. Compounds with this composition were most abundant in the lowest mass fractions, 1 to 3. The total number of M was independent of that of T for $T_{2n}M_{2m}$ and $T_{2n+1}M_{2m+1}$; however, both T and M have to be odd or even simultaneously. In both cases, where m is equal to or less than n, valence requirements dictate the molecule possess a cyclic segment in the overall structure.

$T_{2n}M_{2n}$ and $T_{2n+1}M_{2m+1}$ are reduced to T_nM_n (n = 3, 4, 5, ...) when $m = n$, and molecules with such compositions have a monocyclic structure. From the ESI FTMS data, the smallest member observed in the cyclic family is T_3M_3 and $[T^{Ph}{}_2T^{Me}M^{Vi}{}_3+NH_4]^+$ (m/z 622.17853) was observed. Other members in the cyclic family include T_4M_4, T_5M_5, T_6M_6, and T_7M_7. The two sets of most abundant ions observed in fraction 4 (m/z 782.21472 and m/z 844.23274; m/z 942.25263 and m/z 1004.27093) were assigned to T_4M_4 ($[T^{Ph}{}_2T^{Me}{}_2M^{Vi}{}_4+NH_4]^+$; $[T^{Ph}{}_3T^{Me}M^{Vi}{}_4+NH_4]^+$) and T_5M_5 ($[T^{Ph}{}_3T^{Me}{}_2M^{Vi}{}_5+NH_4]^+$; $[T^{Ph}{}_2T^{Me}{}_3M^{Vi}{}_4+NH_4]^+$), respectively. No larger cyclic compounds were observed. Possible structures for the T_5M_5 composition are shown in Scheme 2.

In other cases, for any given m, a family of $T_{2n}M_{2m}$ or $T_{2n+1}M_{2m+1}$ was likely present. For example, when m = 4, the $T_{2n}M_4$ representation included T_6M_4, T_8M_4, $T_{10}M_4$, etc., and similarly, $T_{2n+1}M_5$ included T_7M_5, T_9M_5, $T_{11}M_5$, etc. Ions observed for these two families are summarized in Table 3 and Table 4, respectively. $T_{2n}M_{2m}$ ($n > m$ and $2m$ = 4, 6, 8, etc.) or $T_{2n+1}M_{2m+1}$ ($n > m$ and $2m + 1$ = 3, 5, 7, etc.) compositions require more than one cyclic structure in the molecule to satisfy the valence requirement. For instance, the $T_{2n}M_4$ composition contains four end groups (M), and one possible way to build the multicyclic structures for this type is to connect T_2M_4 to T_4M_4 at either two adjacent or

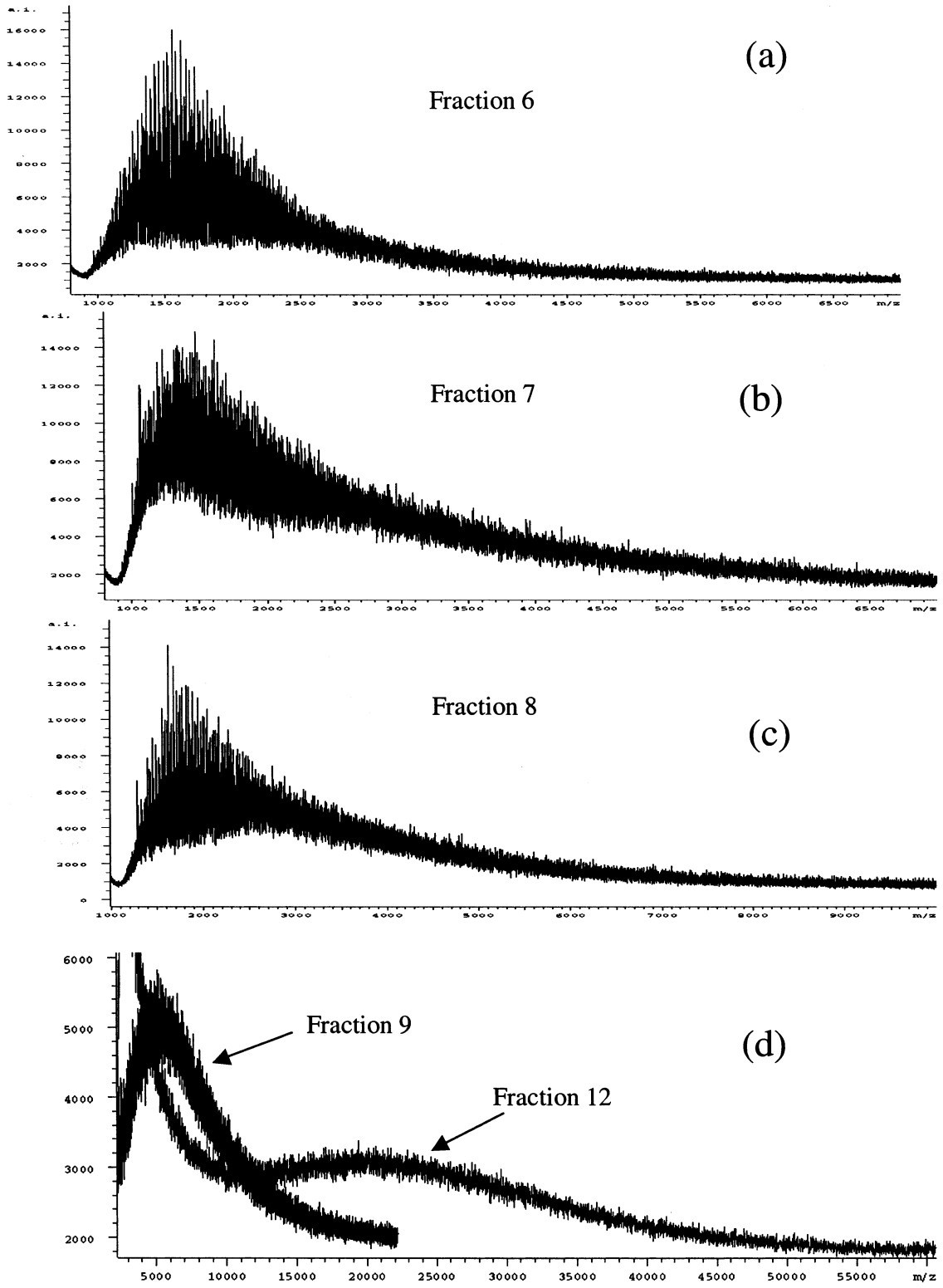

Figure 4. MALDI−TOF MS spectra of (a) fraction 6, (b) fraction 7, (c) fraction 8, and (d) fraction 9 and fraction 12.

nonadjacent vertexes by "elimination" of two M_2 groups. Such stepwise addition would produce a series of compounds (T_6M_4, T_8M_4, $T_{10}M_4$, $T_{12}M_4$, $T_{14}M_4$, $T_{16}M_4$, etc.) with fused-ring structures. If the addition of T_2M_4 always occurred through adjacent vertices, the structures for $T_{2n}M_4$ could be best presented as "ladder" structures, as illustrated in Scheme 3. Such a structure has long been proposed to exist for silsesquioxanes, but not positively proven.[24,25] If T_4M_4 cyclics were combined with T_2M_4 via nonadjacent vertices or a combination of adjacent and nonadjacent vertices (Scheme 4), the resulting structures would contain three-dimensional (partially condensed cage) arrangements. For molecules containing more than six T-silicons (e.g., T_8M_4, $T_{10}M_4$), several types of combinations were likely on the basis of statistic considerations, and only one isomeric structure was presented. It should be emphasized that the structures discussed herein are purely based on valence requirements, not mechanistic considerations. However, it is important to realize that any structure derived by

Table 1. Composition Assignments of ESI FTMS Ions for Fractions 1−3[a]

measured mass $[M + NH_4]^+$	fraction 1 intensity (%)	fraction 2 intensity (%)	fraction 3 intensity (%)	composition assignment	theoretical mass	mass error (ppm)	reduced representation
426.17635	75	14	21	$T^{Ph}M^{Vi}_3$	426.17668	−0.8	TM_3
516.19314	13			$T^{Ph}T^{Me}M^{Vi}_3M^{OMe}$	516.19038	5.3	T_2M_4
524.19966	36	12		$T^{Me}_2M^{Vi}_4$	524.19861	2.0	T_2M_4
578.20693	10	9	8	$T^{Ph}_2M^{Vi}_3M^{OMe}$	578.20603	1.6	T_2M_4
586.21334	100	100	58	$T^{Ph}T^{Me}M^{Vi}_4$	586.21426	−1.6	T_2M_4
622.17853	4	5	5	$T^{Me}T^{Ph}_2M^{Vi}_3$	622.17788	1.1	T_3M_3
648.23070	46	29	100	$T^{Ph}_2M^{Vi}_4$	648.22991	1.2	T_2M_4
658.18418	19	4	4	$T^{Me}_4M^{Vi}_4$	658.18416	0.0	T_4M_4
676.22732	14			$T^{Me}_2T^{Ph}M^{Vi}_4M^{OMe}$	676.22797	−1.0	T_3M_5
684.23998	28	7		$T^{Me}_3M^{Vi}_5$	684.23620	5.5	T_3M_5
720.20214	43	15	31	$T^{Me}_3T^{Ph}M^{Vi}_4$	720.19981	3.2	T_4M_4
738.24594	7	5	13	$T^{Me}T^{Ph}_2M^{Vi}_4M^{OMe}$	738.24362	3.1	T_3M_5
746.25151	57	26	47	$T^{Me}_2T^{Ph}M^{Vi}_5$	746.25184	−0.4	T_3M_5
782.21670	20	11	61	$T^{Me}_2T^{Ph}_2M^{Vi}_4$	782.21546	1.6	T_4M_4
808.26670	12	12	89	$T^{Me}T^{Ph}_2M^{Vi}_5$	808.26749	−1.0	T_3M_5
880.23544	11	6	22	$T^{Me}_4T^{Ph}M^{Vi}_5$	880.23739	−2.2	T_5M_5
906.28950	5	5	8	$T^{Me}_3T^{Ph}M^{Vi}_6$	906.28943	0.1	T_4M_6
916.19968	5	4	30	$T^{Me}_4T^{Ph}_2M^{Vi}_4$	916.20101	−1.5	T_6M_4
942.24772		5	42	$T^{Me}_3T^{Ph}_2M^{Vi}_5$	942.25304	−5.6	T_5M_5
952.16467			16	$T^{Me}_4T^{Ph}_3M^{Vi}_3$	952.16462	0.0	T_7M_3
978.21070			22	$T^{Me}_3T^{Ph}_3M^{Vi}_4$	978.21666	−6.1	T_6M_4

[a] M = $ViMe_2SiO_{1/2}$ (M^{Vi}), or $MeO_{1/2}$; only ions with relative intensities equal to 4% or greater are assigned.

such practice needs to be consistent with the continuity of compositions for each family of molecules.

Compared to $T_{2n}M_4$, the $T_{2n+1}M_3$ composition can be visualized from $T_{2n}M_4$ by removing one T^RM (R = Ph or Me) group, possibly at the end of the structures shown in Schemes 3 and 4 for $T_{2n}M_4$. The $T_{2n+1}M_5$ (T_7M_5, T_9M_5, $T_{11}M_5$, $T_{13}M_5$, $T_{15}M_5$, etc.) compositions can be generated from $T_{2n}M_4$ by adding a T^RM (R = Ph or Me) unit. Such addition would result in ring expansion to form structures containing five-member rings, such as those shown in Scheme 5 for $T_{13}M_5$. Alternatively, adding a T^RM unit to the end of $T_{2n}M_4$ structures would result in cyclic structures with a pendent arm, such as those shown in Scheme 6 for $T_{11}M_5$.

Further addition of TM unit(s) to $T_{2n+1}M_5$ results in a $T_{2n}M_6$ (e.g., T_6M_6, T_8M_6, $T_{10}M_6$, $T_{12}M_6$, etc.) type of composition. Similarly, the structure of these molecules could be viewed as a derivative of $T_{2n+1}M_5$, and it should contain either two five-member rings or one six-member ring in the structure. Alternatively, the TM unit can also be accommodated by replacing an M at the end of $T_{2n+1}M_5$ structure, similar to those shown in Scheme 6.

By taking into account the overall silsesquioxane composition ($T_{0.75}M_{0.25}$), the most probable compositions for $T_{2n}M_{2n}$ or $T_{2n+1}M_{2m+1}$ could be expected to have a T/M ratio at or close to 3. Such species are more likely to be present than species having unfavorable T/M ratios and expectedly reside in the center of $T_{2n}M_{2n}$ or $T_{2n+1}M_{2m+1}$ distributions. For example, the most abundant species observed in the $T_{2n+1}M_3$ and $T_{2n}M_4$ families in fraction 5 were $T^{Ph}_6T^{Me}_3M^{Vi}_3$ (*m/z* 1272.19210, T_9M_3) and $T^{Ph}_6T^{Me}_6M^{Vi}_4$ (*m/z* 1566.22197, $T_{12}M_4$), respectively, all of which had a T/M ratio of 3:1. For the $T_{2n+1}M_5$ family, $T^{Ph}_5T^{Me}_6M^{Vi}_5$ (*m/z* 1530.25708, $T_{11}M_5$, 100%), $T^{Ph}_6T^{Me}_7M^{Vi}_5$ (*m/z* 1726.25696, $T_{13}M_5$, 100%), and $T^{Ph}_6T^{Me}_9M^{Vi}_5$ (*m/z* 1860.24697, $T_{15}M_5$, 83%) were present at comparable levels. Overall, the T/M ratio for oligomeric species in the low-molar-mass fractions were lower than the average value of three due to the presence of individual oligomeric species and their different structural types.

The formation of cage structures (T_8, T_{10}, T_{12}, and iso-T_{12}) from $RSi(OMe)_3$ or $RSiCl_3$ in the trifunctional siloxane systems has been well documented in the literature.[28−30] These structures can often be prepared by base-catalyzed condensation of the hydrolyzates obtained from the acid-catalyzed hydrolysis of organosilanes. Some of these compounds, such as T^{Me}_8, T^{Ph}_8, and T^{Ph}_{12}, have been obtained in almost quantitative yields under optimum conditions. In the $T^{Ph}_{0.35}T^{Me}_{0.40}M^{Vi}_{0.25}$ silsesquioxane system, no fully condensed polyhedra such as T_8 and T_{10} were detected. However, the ESI FTMS spectra did show ions that can be assigned to T_8M_2 ($T^{Ph}_3T^{Me}_5M_2$, *m/z* 926.11219 and T_4PhT_4-MeM^{Vi}_2, *m/z* 988.12938) and $T_{10}M_2$ ($T^{Ph}_5T^{Me}_5M^{Vi}_2$, *m/z* 1184.12543, and $T^{Ph}_6T^{Me}_4M^{Vi}_2$, *m/z* 1246.14508). Such compositions could adopt partially condensed cage structures, and a possible mechanism leading to the formation of T_8M_2 and $T_{10}M_2$ is illustrated in Scheme 7. The partially open cages could form through intramolecular condensation of their ladderlike precursors such as $T_8M'_4$ and $T_{10}M'_4$ where M′ = OH or OMe. In Scheme 8, each vertex represents a T silicon while the R groups are omitted for clarity. The intramolecular condensation can only occur when the hydroxyl groups on the precursor siloxanes are in close proximity and at a favorable orientation. Unreacted hydroxyl groups were deactivated later by capping with M^{Vi} groups. More importantly, this mechanism is consistent with the fused siloxane rings or "ladder" structures proposed for the deactivated potential precursors. A partially condensed open-cage structure is also possible for the T_9M_3 composition (see Scheme 7). However, for other members in the $T_{2n+1}M_3$ family, the open-cage structure is less preferred than the fused ring structure since addition of "TM" would result in continuous cage expansion, and such cagelike structures do not represent the major structural features based upon the results of conformational analysis reported in a following section.

MALDI−TOF MS. Figure 4a−d shows the MALDI mass spectra for fractions 6−9 and 12. Individual species can still be identified for fractions 6−8 due to sufficient mass resolution. Detailed characterization becomes impossible for fractions 9 and 12 due to the high molecular weight species contained in these samples as well as the "peak at every mass" problem for this complex silsesquioxane. The MALDI mass spectrum of fraction 6 was compared to the ESI FTMS spectrum,

Table 2. Composition Assignments of ESI FTMS Ions for Fractions 4 and 5[a]

measured mass $[M+NH_4]^+$	fraction 4 intensity (%)	fraction 5 intensity (%)	most probable comp	theoretical mass	mass error (ppm)	reduced representation	family
648.22965	18		$T^{Ph}_2M^{Vi}_4$	648.22991	−0.4	T_2M_4	T_nM_{n+2}
720.20176	13		$T^{Me}_3T^{Ph}M^{Vi}_4$	720.19981	2.7	T_4M_4	T_nM_n
746.25345	16	5	$T^{Me}_2T^{Ph}M^{Vi}_5$	746.25184	2.2	T_3M_5	T_nM_{n+2}
782.21472	58	9	$T^{Me}_2T^{Ph}_2M^{Vi}_4$	782.21546	−0.9	T_4M_4	T_nM_n
800.25944	13	7	$T^{Ph}_3M^{Vi}_4M^{OMe}$	800.25927	0.2	T_3M_5	T_nM_{n+2}
808.26672	51	9	$T^{Me}T^{Ph}_2M^{Vi}_5$	808.26749	−1.0	T_3M_5	T_nM_{n+2}
844.23274	66	21	$T^{Me}T^{Ph}_3M^{Vi}_4$	844.23111	1.9	T_4M_4	T_nM_n
870.28252	19		$T^{Ph}_3M^{Vi}_5$	870.28314	−0.7	T_3M_5	T_nM_{n+2}
890.14868	22		$T_5{}^{Me}T_2{}^{Ph}M_3{}^{Vi}$	890.14898	−0.3	T_7M_3	$T_{2n+1}M_{2m+1}$
906.24986	13	11	$T^{Ph}_4M^{Vi}_4$	906.24676	3.4	T_4M_4	T_nM_n
916.20202	43	8	$T^{Me}_4T^{Ph}_2M^{Vi}_4$	916.20101	1.1	T_6M_4	$T_{2n}M_{2m}$
926.11219	17	8	$T^{Me}_5T^{Ph}_3M^{Vi}_2$	926.11259	−0.4	T_8M_2	$T_{2n}M_{2m}$
942.25263	67	12	$T^{Me}_3T^{Ph}_2M^{Vi}_5$	942.25304	−0.4	T_5M_5	T_nM_n
952.16494	48	17	$T^{Me}_4T^{Ph}_3M^{Vi}_3$	952.16462	0.3	T_7M_3	$T_{2n+1}M_{2m+1}$
978.21884	62	25	$T^{Me}_3T^{Ph}_3M^{Vi}_4$	978.21666	2.2	T_6M_4	$T_{2n}M_{2m}$
988.12937	30	23	$T^{Me}_4T^{Ph}_4M^{Vi}_2$	988.12869	0.7	T_8M_2	$T_{2n}M_{2m}$
1004.27093	100	37	$T^{Me}_2T^{Ph}_3M^{Vi}_5$	1004.26869	2.2	T_5M_5	T_nM_n
1014.18308	55	50	$T^{Me}_3T^{Ph}_4M^{Vi}_3$	1014.18027	2.8	T_7M_3	$T_{2n+1}M_{2m+1}$
1040.23392	60	50	$T^{Me}_2T^{Ph}_4M^{Vi}_4$	1040.23231	1.5	T_6M_4	$T_{2n}M_{2m}$
1050.14302	20	19	$T^{Me}_3T^{Ph}_5M^{Vi}_2$	1050.14389	−0.8	T_8M_2	$T_{2n}M_{2m}$
1066.28267	45	29	$T^{Me}T^{Ph}_4M^{Vi}_5$	1066.28434	−1.6	T_5M_5	T_nM_n
1076.19724	24	25	$T^{Me}_2T^{Ph}_5M^{Vi}_3$	1076.19592	1.2	T_7M_3	$T_{2n+1}M_{2m+1}$
1076.23430	34		$T^{Me}_5T^{Ph}_2M^{Vi}_5$	1076.23859	−4.0	T_7M_5	$T_{2n+1}M_{2m+1}$
1086.14768	29	13	$T^{Me}_6T^{Ph}_3M^{Vi}_3$	1086.15017	−2.3	T_9M_3	$T_{2n+1}M_{2m+1}$
1102.24427	31	15	$T^{Me}T^{Ph}_5M^{Vi}_4$	1102.24795	−3.3	T_6M_4	$T_{2n}M_{2m}$
1112.20418	52	18	$T^{Me}_5T^{Ph}_3M^{Vi}_4$	1112.20221	1.8	T_8M_4	$T_{2n}M_{2m}$
1138.25289	59	18	$T^{Me}_4T^{Ph}_3M^{Vi}_5$	1138.25424	−1.2	T_7M_5	$T_{2n+1}M_{2m+1}$
1148.16543	51	33	$T^{Me}_5T^{Ph}_4M^{Vi}_3$	1148.16582	−0.3	T_9M_3	$T_{2n+1}M_{2m+1}$
1164.30849	63	26	$T^{Me}_3T^{Ph}_3M^{Vi}_6$	1164.30628	1.9	T_6M_6	T_nM_n
1174.21692	74	44	$T^{Me}_4T^{Ph}_4M^{Vi}_4$	1174.21786	−0.8	T_8M_4	$T_{2n}M_{2m}$
1184.12543	24	19	$T^{Me}_5T^{Ph}_5M^{Vi}_2$	1184.12944	−3.4	$T_{10}M_2$	$T_{2n}M_{2m}$
1200.27053	67	41	$T^{Me}_3T^{Ph}_4M^{Vi}_5$	1200.26989	0.5	T_7M_5	$T_{2n+1}M_{2m+1}$
1210.18010	43	47	$T^{Me}_4T^{Ph}_5M^{Vi}_3$	1210.18147	−1.1	T_9M_3	$T_{2n+1}M_{2m+1}$
1226.32037	36	32	$T^{Me}_2T^{Ph}_4M^{Vi}_6$	1226.32192	−1.3	T_6M_6	T_nM_n
1236.23340	50	58	$T^{Me}_3T^{Ph}_5M^{Vi}_4$	1236.23350	−0.1	T_8M_4	$T_{2n}M_{2m}$
1246.14475		22	$T^{Me}_4T^{Ph}_6M^{Vi}_2$	1246.14508	−0.3	$T_{10}M_2$	$T_{2n}M_{2m}$
1246.18748	32		$T^{Me}_2T^{Ph}_3M^{Vi}_4$	1246.18776	−0.2	$T_{10}M_4$	$T_{2n}M_{2m}$
1262.28581	45	59	$T^{Me}_2T_5PhM_5{}^{Vi}$	1262.28554	0.2	T_7M_5	$T_{2n+1}M_{2m+1}$
1272.19210	37	63	$T^{Me}_3T^{Ph}_6M^{Vi}_3$	1272.19712	−3.9	T_9M_3	$T_{2n+1}M_{2m+1}$
1272.23510	62	0	$T^{Me}_6T^{Ph}_3M^{Vi}_5$	1272.23979	−3.7	T_9M_5	$T_{2n+1}M_{2m+1}$
1282.14975	35	37	$T^{Me}_7T^{Ph}_4M^{Vi}_3$	1282.15137	−1.3	$T_{11}M_3$	$T_{2n+1}M_{2m+1}$
1298.24400	20	27	$T^{Me}_2T^{Ph}_6M^{Vi}_4$	1298.24915	−4.0	T_8M_4	$T_{2n}M_{2m}$
1298.29473	45		$T^{Me}_5T^{Ph}_3M^{Vi}_6$	1298.29182	2.2	T_8M_6	$T_{2n}M_{2m}$
1308.20302	47	39	$T^{Me}_4T^{Ph}_4M^{Vi}_4$	1308.20340	−0.3	T_8M_4	$T_{2n}M_{2m}$
1324.34060	20	15	$T^{Me}_4T^{Ph}_3M^{Vi}_7$	1324.34386	−2.5	T_7M_7	T_nM_n
1334.20938	50	37	$T^{Me}_2T^{Ph}_7M^{Vi}_3$	1334.21277	−2.5	T_9M_3	$T_{2n+1}M_{2m+1}$
1344.12161	29	34	$T^{Me}_3T^{Ph}_8M^{Vi}_1$	1344.12435	−2.0	$T_{11}M_1$	$T_{2n+1}M_{2m+1}$
1360.30531	49	32	$T^{Me}_4T^{Ph}_4M^{Vi}_6$	1360.30747	−1.6	T_8M_6	$T_{2n}M_{2m}$
1370.21814	49	53	$T^{Me}_5T^{Ph}_5M^{Vi}_4$	1370.21905	−0.7	$T_{10}M_4$	$T_{2n}M_{2m}$
1396.27153	45	52	$T^{Me}_4T^{Ph}_5M^{Vi}_5$	1396.27109	0.3	T_9M_5	$T_{2n+1}M_{2m+1}$
1406.17999	36	45	$T^{Me}_5T^{Ph}_6M^{Vi}_3$	1406.18267	−1.9	$T_{11}M_3$	$T_{2n+1}M_{2m+1}$
1422.32595	29	28	$T^{Me}_3T^{Ph}_5M^{Vi}_6$	1422.32312	2.0	T_8M_6	$T_{2n}M_{2m}$
1432.23544	41	52	$T^{Me}_4T^{Ph}_6M^{Vi}_4$	1432.23470	0.5	$T_{10}M_4$	$T_{2n}M_{2m}$
1442.18504	22	25	$T^{Me}_8T^{Ph}_4M^{Vi}_4$	1442.18896	−2.7	$T_{12}M_4$	$T_{2n}M_{2m}$
1458.28707	32	33	$T^{Me}_3T^{Ph}_6M^{Vi}_5$	1458.28674	0.2	T_9M_5	$T_{2n+1}M_{2m+1}$
1468.24022	39	39	$T^{Me}_7T^{Ph}_4M^{Vi}_5$	1468.24099	−0.5	$T_{11}M_5$	$T_{2n+1}M_{2m+1}$
1494.29001	38	40	$T^{Me}_6T^{Ph}_4M^{Vi}_6$	1494.29302	−2.0	$T_{10}M_6$	$T_{2n}M_{2m}$
1504.20296	36	47	$T^{Me}_7T^{Ph}_5M^{Vi}_4$	1504.20460	−1.1	$T_{12}M_4$	$T_{2n}M_{2m}$
1530.25708	59	100	$T^{Me}_6T^{Ph}_5M^{Vi}_5$	1530.25664	0.3	$T_{11}M_5$	$T_{2n+1}M_{2m+1}$
1540.16465	30	46	$T^{Me}_7T^{Ph}_6M^{Vi}_3$	1540.16822	−2.3	$T_{13}M_3$	$T_{2n+1}M_{2m+1}$
1556.30675	58	96	$T^{Me}_5T^{Ph}_5M^{Vi}_6$	1556.30867	−1.2	$T_{10}M_6$	$T_{2n}M_{2m}$
1566.22197	38	66	$T^{Me}_6T^{Ph}_6M^{Vi}_4$	1566.22025	1.1	$T_{12}M_4$	$T_{2n}M_{2m}$
1582.35691	21	35	$T^{Me}_4T^{Ph}_5M^{Vi}_7$	1582.36070	−2.4	T_9M_7	$T_{2n+1}M_{2m+1}$
1592.27041	41	73	$T^{Me}_5T^{Ph}_6M^{Vi}_5$	1592.27229	−1.2	$T_{11}M_5$	$T_{2n+1}M_{2m+1}$
1602.17590		48	$T^{Me}_6T^{Ph}_7M^{Vi}_3$	1602.18386	5.0	$T_{13}M_3$	$T_{2n+1}M_{2m+1}$
1602.22604	35		$T^{Me}_9T^{Ph}_4M^{Vi}_5$	1602.22654	−0.3	$T_{13}M_5$	$T_{2n+1}M_{2m+1}$
1618.32484	32	65	$T^{Me}_4T^{Ph}_6M^{Vi}_6$	1618.32432	0.3	$T_{10}M_6$	$T_{2n}M_{2m}$
1628.23391	39	50	$T^{Me}_5T^{Ph}_7M^{Vi}_4$	1628.23590	−1.2	$T_{12}M_4$	$T_{2n}M_{2m}$
1638.18975	25	42	$T^{Me}_9T^{Ph}_5M^{Vi}_4$	1638.19014	−0.2	$T_{14}M_4$	$T_{2n}M_{2m}$
1654.28198	44	66	$T^{Me}_4T^{Ph}_7M^{Vi}_5$	1654.28783	−3.5	$T_{11}M_5$	$T_{2n+1}M_{2m}$
1664.24220	41	92	$T^{Me}_8T^{Ph}_5M^{Vi}_5$	1664.24219	0.0	$T_{13}M_5$	$T_{2n+1}M_{2m+1}$
1690.29205	52	94	$T^{Me}_7T^{Ph}_5M^{Vi}_6$	1690.29422	−1.3	$T_{12}M_6$	$T_{2n}M_{2m}$
1700.20794	30	63	$T^{Me}_8T^{Ph}_6M^{Vi}_4$	1700.20580	1.3	$T_{14}M_4$	$T_{2n}M_{2m}$
1716.34929	28	65	$T^{Me}_6T^{Ph}_5M^{Vi}_7$	1716.34626	1.8	$T_{11}M_7$	$T_{2n+1}M_{2m+1}$
1726.25696	40	100	$T^{Me}_7T^{Ph}_6M^{Vi}_5$	1726.25784	−0.5	$T_{13}M_5$	$T_{2n+1}M_{2m+1}$

Table 2. Continued

measured mass $[M+NH_4]^+$	fraction 4 intensity (%)	fraction 5 intensity (%)	most probable comp	theoretical mass	mass error (ppm)	reduced representation	family
1752.30947	28	75	$T^{Me}_6T^{Ph}_6M^{Vi}_6$	1752.30987	−0.2	$T_{12}M_6$	$T_{2n}M_{2m}$
1762.21079	30	63	$T^{Me}_7T^{Ph}_7M^{Vi}_4$	1762.22144	−6.0	$T_{14}M_4$	$T_{2n}M_{2m}$
1778.36432	23	66	$T^{Me}_5T^{Ph}_6M^{Vi}_7$	1778.36191	1.4	$T_{11}M_7$	$T_{2n+1}M_{2m+1}$
1788.26808	32	61	$T^{Me}_6T^{Ph}_7M^{Vi}_5$	1788.27348	−3.0	$T_{13}M_5$	$T_{2n+1}M_{2m+1}$
1798.22552	27	61	$T^{Me}_{10}T^{Ph}_5M^{Vi}_5$	1798.22774	−1.2	$T_{15}M_5$	$T_{2n+1}M_{2m+1}$
1814.32382	28	63	$T^{Me}_5T^{Ph}_7M^{Vi}_6$	1814.32551	−0.9	$T_{12}M_6$	$T_{2n}M_{2m}$
1824.27982	36	73	$T^{Me}_9T^{Ph}_5M^{Vi}_6$	1824.27977	0.0	$T_{14}M_6$	$T_{2n}M_{2m}$
1850.33117	26	55	$T^{Me}_8T^{Ph}_5M^{Vi}_7$	1850.33181	−0.3	$T_{13}M_7$	$T_{2n+1}M_{2m+1}$
1860.24697	26	83	$T^{Me}_9T^{Ph}_6M^{Vi}_5$	1860.24339	1.9	$T_{15}M_5$	$T_{2n+1}M_{2m+1}$
1886.29713	30	81	$T^{Me}_8T^{Ph}_6M^{Vi}_6$	1886.29542	0.9	$T_{14}M_6$	$T_{2n}M_{2m}$
1912.33712	20	46	$T^{Me}_7T^{Ph}_6M^{Vi}_7$	1912.34746	−5.4	$T_{13}M_7$	$T_{2n+1}M_{2m+1}$
1922.29796	26	66	$T^{Me}_{11}T^{Ph}_4M^{Vi}_7$	1922.30171	−2.0	$T_{15}M_7$	$T_{2n+1}M_{2m+1}$
1948.31357	22	77	$T^{Me}_7T^{Ph}_7M^{Vi}_6$	1948.31106	1.3	$T_{14}M_6$	$T_{2n}M_{2m}$
1984.31831	17	34	$T^{Me}_{10}T^{Ph}_5M^{Vi}_7$	1984.31736	0.5	$T_{15}M_7$	$T_{2n+1}M_{2m+1}$
2020.28602	20	65	$T^{Me}_{10}T^{Ph}_6M^{Vi}_6$	2020.28096	2.5	$T_{16}M_6$	$T_{2n}M_{2m}$

[a] M = $ViMe_2SiO_{1/2}$ (M^{Vi}), or $MeO_{1/2}$.

Scheme 1. Classification of Species in the $(PhSiO_{3/2})_{0.35}(MeSiO_{3/2})_{0.40}(Me_2ViSiO_{1/2})_{0.25}$ Resin

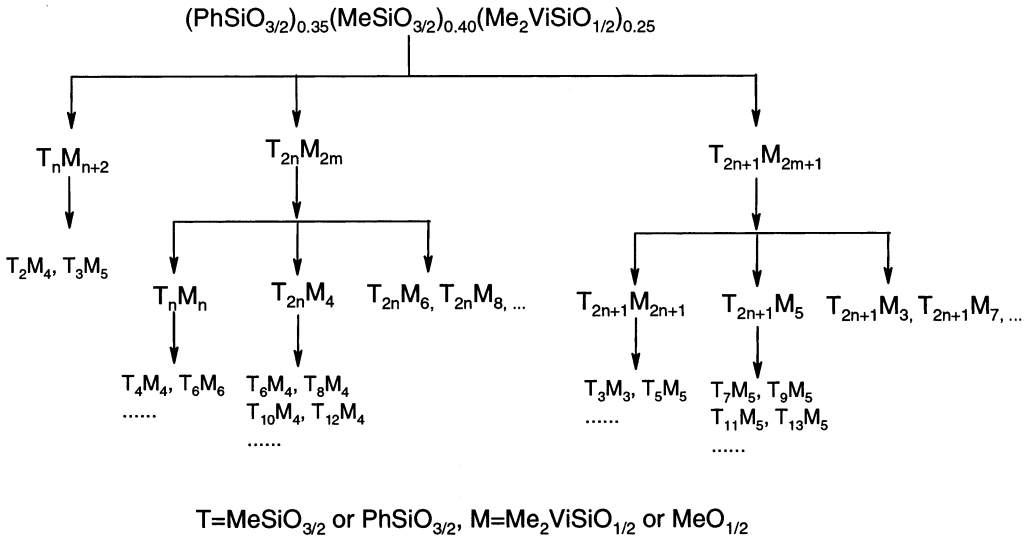

Scheme 2. Possible Structures for T_5M_5

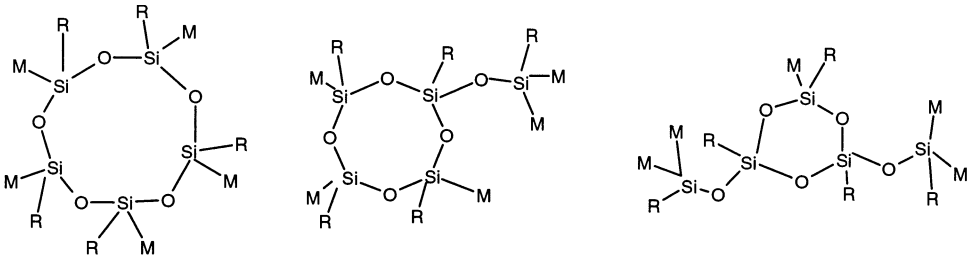

Table 3. A List of Ions Observed for $T_{2n}M_4$ (n = 3−7)

composition	observed molecular ions $[M+NH_4]^+$: m/z (composition)
T_6M_4	1164 ($T^{Ph}_6M^{Vi}_4$), 1102 ($T^{Ph}_5T^{Me}M^{Vi}_4$), 1040 ($T^{Ph}_4T^{Me}_2M^{Vi}_4$), 978 ($T^{Ph}_3T^{Me}_3M^{Vi}_4$), 916 ($T^{Ph}_2T^{Me}_4M^{Vi}_4$)
T_8M_4	1298 ($T^{Ph}_6T^{Me}_2M^{Vi}_4$), 1236 ($T^{Ph}_5T^{Me}_3M^{Vi}_4$), 1174 ($T^{Ph}_4T^{Me}_4M^{Vi}_4$), 1112 ($T^{Ph}_3T^{Me}_5M^{Vi}_4$)
$T_{10}M_4$	1432 ($T^{Ph}_6T^{Me}_4M^{Vi}_4$), 1370 ($T^{Ph}_5T^{Me}_5M^{Vi}_4$), 1308 ($T^{Ph}_4T^{Me}_6M^{Vi}_4$), 1246 ($T^{Ph}_3T^{Me}_7M^{Vi}_4$)
$T_{12}M_4$	1628 ($T^{Ph}_7T^{Me}_5M^{Vi}_4$), 1566 ($T^{Ph}_6T^{Me}_6M^{Vi}_4$), 1504 ($T^{Ph}_5T^{Me}_7M^{Vi}_4$), 1442 ($T^{Ph}_4T^{Me}_8M^{Vi}_4$)
$T_{14}M_4$	1762 ($T^{Ph}_7T^{Me}_7M^{Vi}_4$), 1700 ($T^{Ph}_6T^{Me}_8M^{Vi}_4$), 1638 ($T^{Ph}_5T^{Me}_9M^{Vi}_4$)

and common species and similar relative distributions were observed. Since FTMS provides better quality data, detailed composition analysis based upon the MALDI data was not attempted. The molar mass distributions were calculated for fractions 6−9, and the results were compared to the values determined by SEC.

In summary, a large number of individual silsesquioxane molecules were identified by ESI FTMS and classified into three major categories (T_nM_{n+2}, $T_{2n+1}M_{2m+1}$, and $T_{2n}M_{2m}$) on the basis of structural compositions. Possible structures for individual identified species are proposed on the basis of valence requirements for the fundamental structural building units and T/M ratios. The T_nM_{n+2} representation obviously adopts a linear or branched structure whereas T_nM_{n+2} and $T_{2n+1}M_{2m+1}$ can be best represented by fused rings connecting through either adjacent or nonadjacent vertices. In the following sections, NMR results and other analytical data are

Scheme 3. Structures Derived from Connection between Adjacent Vertices for T_nM_4 Compositions

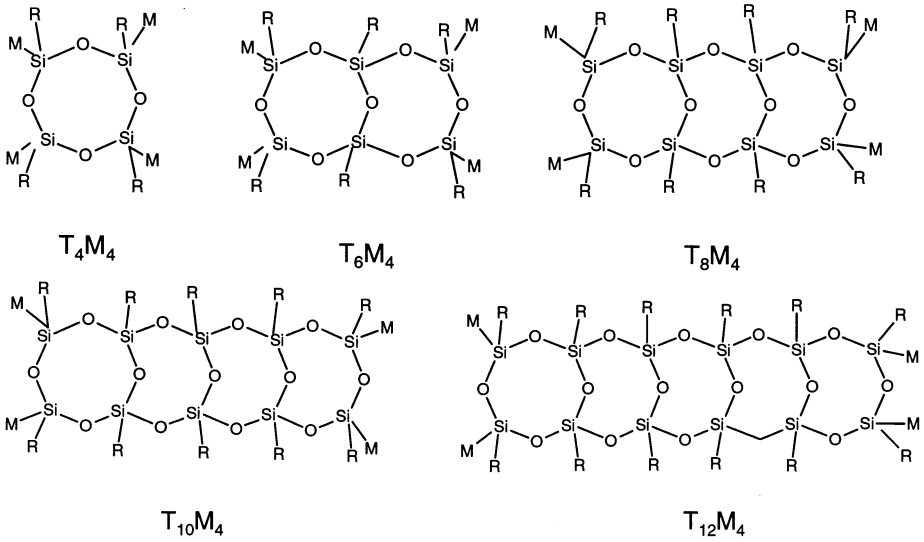

Scheme 4. Structures Derived from Connections between Nonadjacent Vertices or a Combination of Adjacent and Nonadjacent Vertices

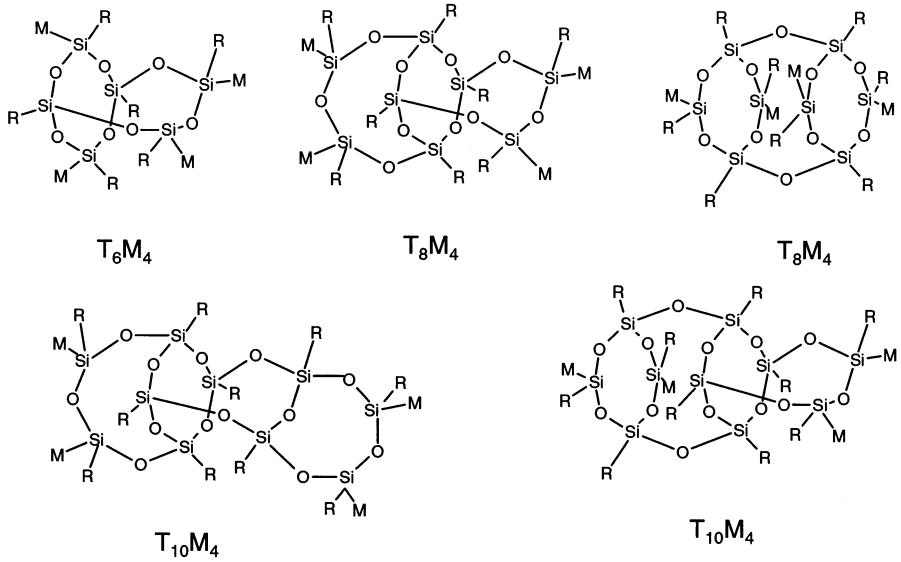

Scheme 5. Possible Structures for $T_{13}M_5$

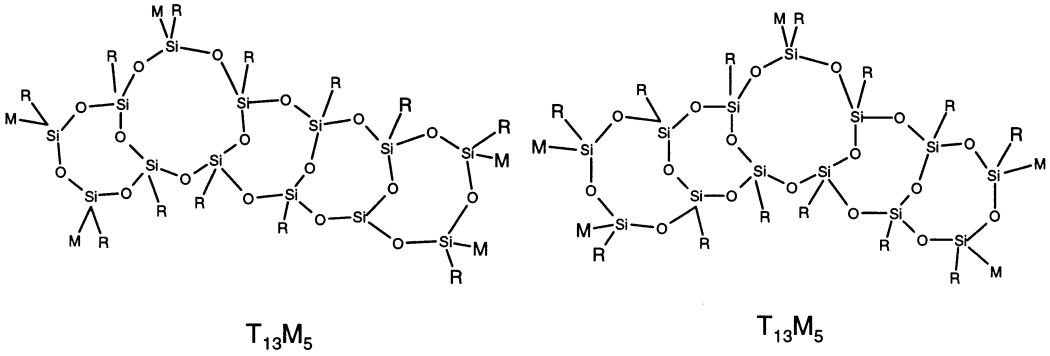

discussed, providing further understanding of the structural features for this $T^{Ph}_{0.35}T^{Me}_{0.40}M^{Vi}_{0.25}$ silsesquioxane.

NMR Analysis. The compositions of the fractions were determined from ^{1}H NMR spectra by integrating the resonances arising from $C_6H_5SiO_{3/2}$, (6.8−8.0 ppm), $CH_3SiO_{3/2}$ (0−1.0 ppm), and $(CH_3)_2(CH_2{=}CH)SiO_{1/2}$ (5−6.5 ppm). These results are presented in Table 5. The mole fractions of $PhSiO_{3/2}$, $MeSiO_{3/2}$, and $Me_2ViSiO_{1/2}$ are also plotted in Figure 5 with respect to the molecular weight (M_n) of each fraction. The $Me_2ViSiO_{1/2}$ content was higher in the low-molar-mass fractions (fractions 1−4); however, it remained constant (∼0.2) for fractions 8−13. In contrast, the $PhSiO_{3/2}$ and $MeSiO_{3/2}$ content increased with molecular weight and attained constant values after fraction 8. The T/M ratios listed in Table 5

Scheme 6. Alternative Structures for $T_{11}M_5$ Compositions

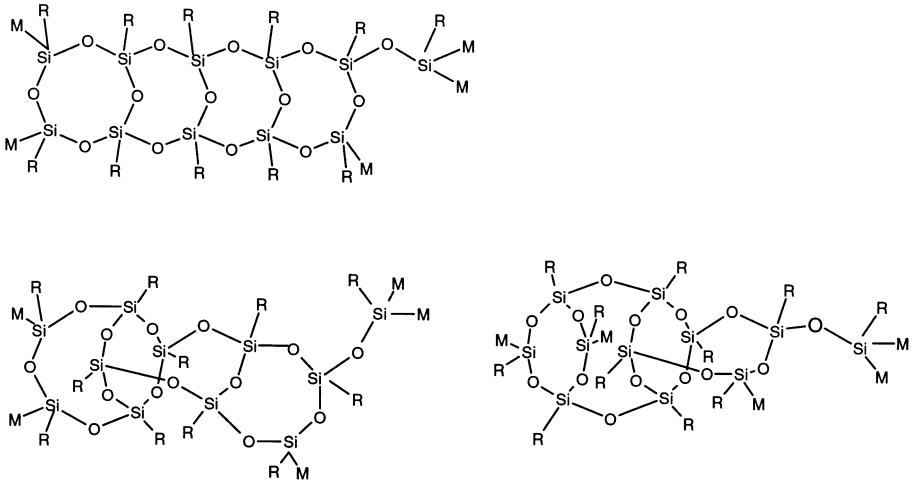

Scheme 7. Possible Mechanism for the Formation of T_8M_2, $T_{10}M_2$, and T_9M_3

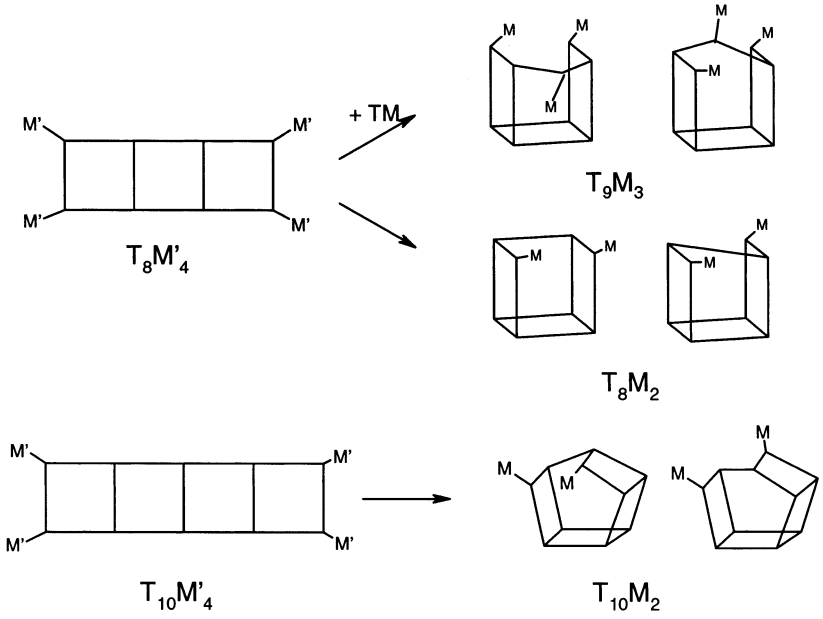

Scheme 8. Four Coordination Spheres for T^{Ph} and T^{Me}

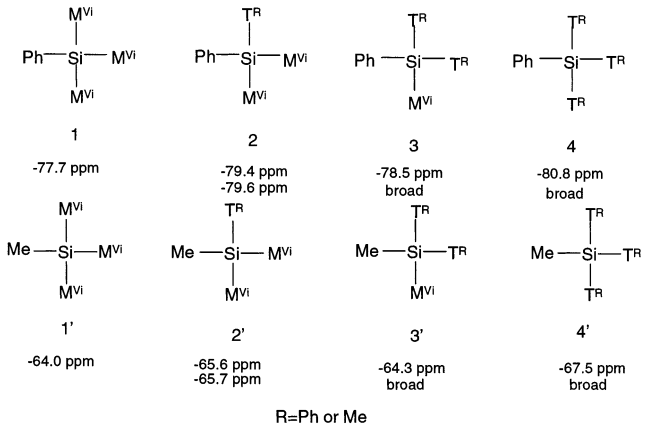

provided direct evidence of compositional inhomogeneity observed for the low-molar-mass fractions, and their low T/M values were consistent with the presence of oligomeric species observed by MS techniques.

The ^{29}Si NMR spectrum of unfractionated $(PhSiO_{3/2})_{0.35}(MeSiO_{3/2})_{0.40}(Me_2ViSiO_{1/2})_{0.25}$ displayed three groups of resonances between 2 and −5, −60 and −70, and −75 and −85 ppm, corresponding to M^{Me2Vi}, $T^{Me}{}_3$, and $T^{Ph}{}_3$ silicons, respectively. The weak resonances at −57.5 and −70.5 ppm were attributed to T_2 silicons, $Me(ZO)SiO_{2/2}$ and $Ph(ZO)SiO_{2/2}$ (Z = H or Me), respectively. The T_3 resonance showed a multiplet pattern that could be attributed to monomer sequence distribution of $Me_2ViSiO_{1/2}$, $PhSiO_{3/2}$, and $MeSiO_{3/2}$. To help interpret the NMR data, three additional resins, $(PhSiO_{3/2})_{0.75}(Me_2ViSiO_{1/2})_{0.25}$,[42] $(MeSiO_{3/2})_{0.75}(Me_2ViSiO_{1/2})_{0.25}$,[43] and

Table 4. A List of Ions Observed for $T_{2n+1}M_5$ (n = 3−7)

composition	observed molecular ions $[M+NH_4]^+$: m/z (composition)
T_7M_5	1262 ($T^{Ph}{}_5T^{Me}{}_2M^{Vi}{}_5$), 1200 ($T^{Ph}{}_4T^{Me}{}_3M^{Vi}{}_5$), 1138 ($T^{Ph}{}_3T^{Me}{}_4M^{Vi}{}_5$)
T_9M_5	1458 ($T^{Ph}{}_6T^{Me}{}_3M^{Vi}{}_5$), 1396 ($T^{Ph}{}_5T^{Me}{}_4M^{Vi}{}_5$), 1334 ($T^{Ph}{}_4T^{Me}{}_5M^{Vi}{}_5$), 1272 ($T^{Ph}{}_3T^{Me}{}_6M^{Vi}{}_5$)
$T_{11}M_5$	1654 ($T^{Ph}{}_7T^{Me}{}_4M^{Vi}{}_5$), 1592 ($T^{Ph}{}_6T^{Me}{}_5M^{Vi}{}_5$), 1530 ($T^{Ph}{}_5T^{Me}{}_6M^{Vi}{}_5$), 1468 ($T^{Ph}{}_4T^{Me}{}_7iM^{V}{}_5$) 1406 ($T^{Ph}{}_3T^{Me}{}_8M^{Vi}{}_5$)
$T_{13}M_5$	1788 ($T^{Ph}{}_7T^{Me}{}_6M^{Vi}{}_5$), 1726 ($T^{Ph}{}_6T^{Me}{}_7M^{Vi}{}_5$), 1664 ($T^{Ph}{}_5T^{Me}{}_8M^{Vi}{}_5$), 1602 ($T^{Ph}{}_4T^{Me}{}_9M^{Vi}{}_5$)
$T_{15}M_5$	1860 ($T^{Ph}{}_6T^{Me}{}_9M^{Vi}{}_5$), 1798 ($T^{Ph}{}_5T^{Me}{}_{10}M^{Vi}{}_5$)

Table 5. Compositions Determined from ^{1}H NMR Spectra for a $(PhSiO_{3/2})_x(MeSiO_{3/2})_y(ViMe_2SiO_{1/2})_z$ Resin and Its Fractions

	x	*y*	*z*	T/M ratio
theoretical	0.350	0.400	0.250	3.0
sample	0.353	0.426	0.223	3.5
SFE control	0.364	0.406	0.231	3.3
F1	0.167	0.262	0.570	0.75
F2	0.190	0.305	0.504	0.98
F3	0.269	0.372	0.357	1.8
F4	0.338	0.352	0.310	2.2
F5	0.356	0.405	0.239	3.2
F6	0.366	0.409	0.225	3.4
F7	0.382	0.398	0.220	3.5
F8	0.377	0.415	0.208	3.8
F9	0.378	0.428	0.194	4.2
F10	0.380	0.441	0.179	4.6
F11	0.376	0.446	0.177	4.6
F12	0.386	0.432	0.182	4.5
F13	0.387	0.433	0.180	4.6

$(PhSiO_{3/2})_{0.45}(MeSiO_{3/2})_{0.30}(Me_2ViSiO_{1/2})_{0.25}$,[44] were prepared and further purified by solvent precipitation to remove the oligomers and vacuum-dried before NMR analysis. The ^{29}Si NMR spectra of these purified high-molecular-weight materials are shown in Figure 6. For the $(PhSiO_{3/2})_{0.75}(Me_2ViSiO_{1/2})_{0.25}$ resin, two groups of resonances resulting from $PhSiO_{3/2}$ (T^{Ph}) and $ViMe_2SiO_{1/2}$ (M^{Vi}) silicons at between −75 and −84 ppm and −1.5 ppm were observed. The ^{29}Si NMR spectrum of the $(MeSiO_{3/2})_{0.75}(Me_2ViSiO_{1/2})_{0.25}$ resin showed resonances arising from $MeSiO_{3/2}$ (T^{Me}) and $ViMe_2SiO_{1/2}$ (M^{Vi}) silicons between −64 and −70 ppm and at −2.8 ppm, respectively. Three major peaks that can be attributed to $PhSiO_{3/2}$ (T^{Ph}), $MeSiO_{3/2}$ (T^{Me}), and $ViMe_2SiO_{1/2}$ (M^{Vi}) silicons between −75 and −84 ppm, −64 and −70 ppm, and, 0 and −4 ppm are observed in the spectrum of the $(PhSiO_{3/2})_{0.45}(MeSiO_{3/2})_{0.30}(Me_2ViSiO_{1/2})_{0.25}$ resin. The weak but broad resonances around −55.8 and −70.0 ppm in all three spectra were assigned to $MeSi(ZO)SiO_{2/2}$ and $PhSi(ZO)SiO_{2/2}$ silicon nuclei, respectively. The "doublet" patterns for the $PhSiO_{3/2}$ (T^{Ph}) and $MeSiO_{3/2}$ (T^{Me}) silicon resonances were observed in all three materials, regardless of the compositions. This is a very important observation that implies that the neighboring T silicon (T^{Me} or T^{Ph}) has a negligible effect on the NMR doublet pattern for the T silicon due to the broad nature of these resonances. The "doublet" feature (ca. 2 ppm apart) observed in the ^{29}Si NMR of the current silsesquioxane fractions did not result from T^{Me} and T^{Ph} distributions, but from T and M combinations.

As mentioned before, each group of T_3 resonances for the $(PhSiO_{3/2})_{0.35}(MeSiO_{3/2})_{0.40}(Me_2ViSiO_{1/2})_{0.25}$ silsesquioxane and its fractions also contained more than one peak, and examination of relative intensities of these peaks could provide information on connectivity and structural correlation between low- and high-molecular-weight materials. Schematic illustrations of the coordination spheres for T^R and peak assignments are shown in Scheme 8. The ^{29}Si NMR spectrum of fraction 1 in Figure 7a shows resonances consistent with the presence of $RSi(OSiMe_2Vi)_3$ (TM_3), $(Me_2ViSiO)_2RSiOSiR'(OSiMe_2Vi)_2$, or dimers ($T_2M_4$). The strongest peak at −77.7 ppm results from T^{Ph} silicon nuclei in $PhSi(OSiMe_2Vi)_3$ ($T^{Ph}M^{Vi}_3$, **1**), and the two smaller peaks at −79.4 and −79.6 ppm are assigned to the T^{Ph} silicon nuclei in $T^{Ph}_2M^{Vi}_4$ (**2**) or $T^{Me}T^{Ph}M^{Vi}_4$ (**2**) as well as oligomers. Similarly, the strong peak at −64.0 ppm results from T^{Me} silicon $MeSi(OSiMe_2Vi)_3$ ($T^{Me}M^{Vi}_3$, **1′**), and two peaks at −65.6 and −65.7 ppm are from T^{Me} silicons in $T^{Me}_2M^{Vi}_4$ (**2′**), $T^{Me}T^{Ph}M^{Vi}_4$ (**2′**), or other oligomeric species. These assignments of $T^RM^{Vi}_3$ were confirmed by an independent NMR analysis of $PhSi(OSiMe_2Vi)_3$ and $MeSi(OSiMe_2Vi)_3$ obtained commercially.[45]

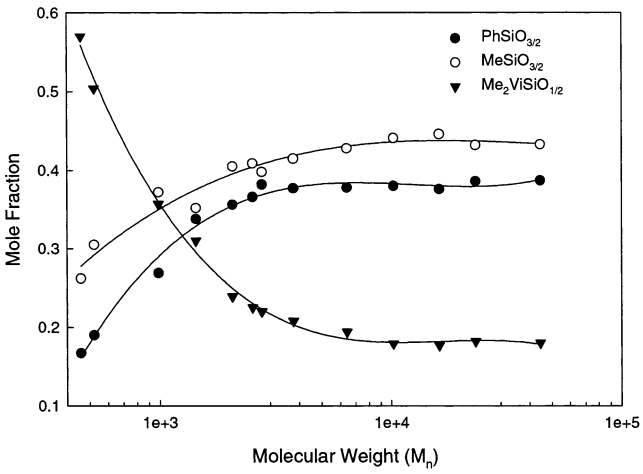

Figure 5. Mole fraction of $PhSiO_{3/2}$, $MeSiO_{3/2}$, and $Me_2ViSiO_{1/2}$ vs molecular weight of the individual fraction (M_n for fraction 1 to 2 from SEC with PS standard while the parent resin and 3 to 13 from SEC with triple detection).

The ^{29}Si NMR spectrum of fraction 2 (Figure 7b) showed strong peaks for dimers and oligomers while the peak intensity for monomers decreased. This trend was consistent with the GC-MS results, which also indicated higher intensities of dimer peaks in fraction 2. The ^{29}Si NMR spectrum of fraction 3 (Figure 7c) shows significant changes compared to fractions 1 and 2. In the T^{Ph} region, two new broad peaks at −78.5 (**3**) and −80.8 ppm (**4**) are observed, in addition to relatively weak signals arising from TM_3 and T_2M_4. These two new peaks were attributed to the T^{Ph} silicons connected to more than one other T silicon, as shown in Scheme 8. The broad nature of these resonances may reflect differences in binding environment due to the statistic distribution of T units (T^{Ph}, T^{Me}). Similarly, the two new peaks at −64.3 (**3′**) and −67.5 ppm (**4′**) were assigned to T^{Me} surrounded by more than one T group.

The ^{29}Si NMR spectra of fractions 4, 5, and 13 (see Figure 8) indicate a diminishing of peaks corresponding to **1**, **1′**, **2**, and **2′** and a growth of resonances corresponding to **3**, **3′**, **4**, and **4′**. It is noteworthy that the peak intensities at −67.5 (**4′**) and −80.8 ppm (**4**) increased rapidly from fraction 4 to fraction 5 but then decreased from fraction 5 to 13. The opposite trend was observed for resonances at −64.3 (**3′**) and −78.5 ppm (**3**). It should be noted that no detectable **2** or **2′** groups were observed by ^{29}Si NMR spectra. This suggests that structures with pendent arms such as those shown in Schemes 2 and 6 are less likely; i.e., structures shown in Scheme 5 are more probable.The chemical shifts for resonances assigned to **3**, **3′**, **4**, and **4′** structures were consistent with a T^R silicon involved in cyclic structures. The difference in chemical shift between the **1** (**1′**) and **2** (**2′**), **2** (**2′**) and **3** (**3′**), **3**(**3′**) and **4**(**4′**), resulting from sequential attachment of $Me_2ViSiO_{1/2}$ to T silicon were not the same, and in fact, the resonances attributed to **3** and **3′** appeared at lower field. Such a shift to low field for silicons constrained in ring or cage structures has been observed in silsesquioxane systems.[46] The assignment of the broad peak at −78.5 ppm to the $T^{Ph}T^R_2M^{Vi}$ silicon involved in ring structures was further supported by NMR analysis the cyclic compound, $T^{Ph}_4M^{Vi}_4$, synthesized via an independent route.[47] The model com-

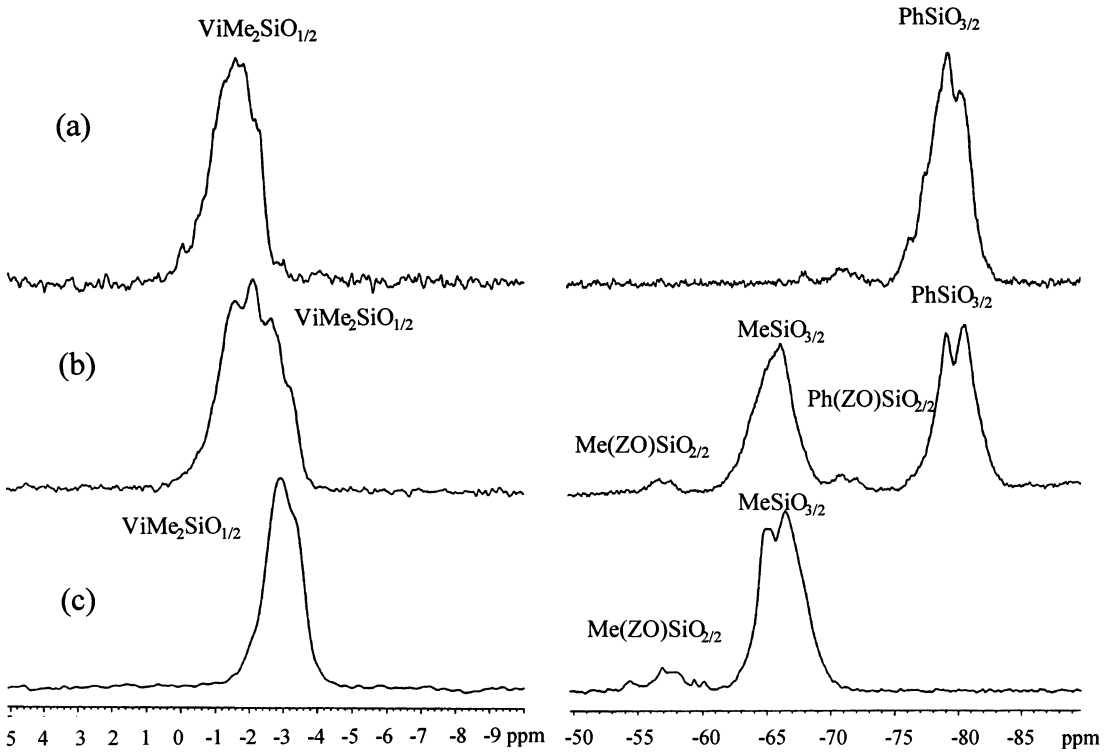

Figure 6. ^{29}Si NMR spectra of model resins (a) $(PhSiO_{3/2})_{0.75}(Me_2ViSiO_{1/2})_{0.25}$, (b) $(PhSiO_{3/2})_{0.45}(MeSiO_{3/2})_{0.30}(Me_2ViSiO_{1/2})_{0.25}$, and (c) $(MeSiO_{3/2})_{0.75}(Me_2ViSiO_{1/2})_{0.25}$.

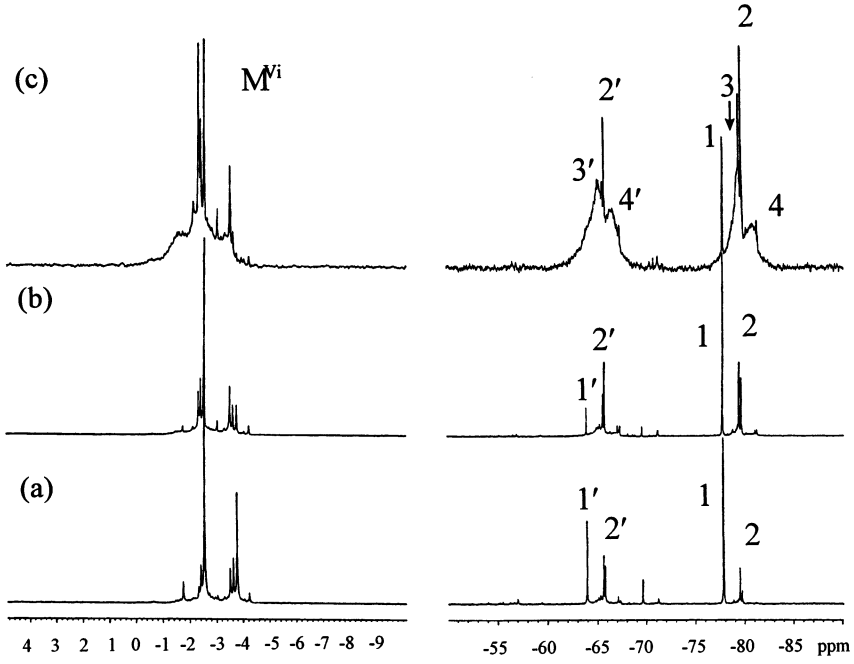

Figure 7. ^{29}Si NMR spectrum of (a) fraction 1, (b) fraction 2, and (c) fraction 3.

pound showed a resonance with a similar chemical shift (−78.4 ppm).

To determine the relative mole fractions of T(M) (**3** and **3′**) and T (**4** and **4′**) units, deconvolution of the ^{29}Si NMR spectra of the fractions was performed using Varian's NMR fitting program. While the pure Lorentzian line fitting was assumed in the deconvolution procedure, the frequency (hertz), intensity, and line width (in hertz at half-height) of the peaks at −64.3 (**3′**), −67.50 (**4′**), −78.5 (**3**), and −80.8 ppm (**4**) were included to calculate the spectrum. A linear baseline correction was added to the fit to avoid errors produced by baseline offsets. The resulting integration values were used for calculating the mole percentage. For illustrative purposes, the original spectrum, the calculated spectrum, and each component line for fraction 5 are shown in Figure 9**.** The mole percentages of T(M) (**3** and **3′**) and T (**4** and **4′**) units in fractions 4, 5, 6, and 13 determined by deconvolution are summarized in Table 6, along with the T_2(OZ) and M^{Vi} content determined from the ^{29}Si NMR spectra. It was assumed that the possibility of having one M^{Vi} group connected to a T_2 and T_3 silicon

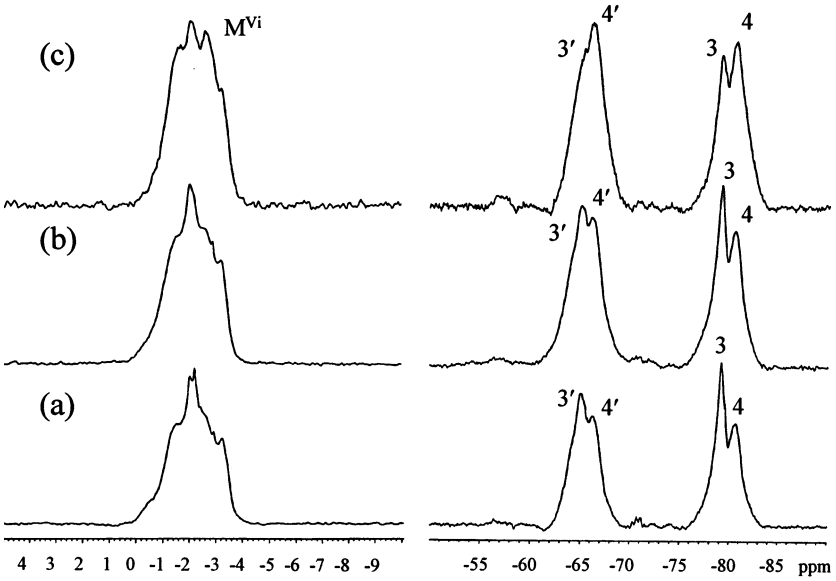

Figure 8. ^{29}Si NMR spectrum of (a) fraction 4, (b) fraction 5, and (c) fraction 13.

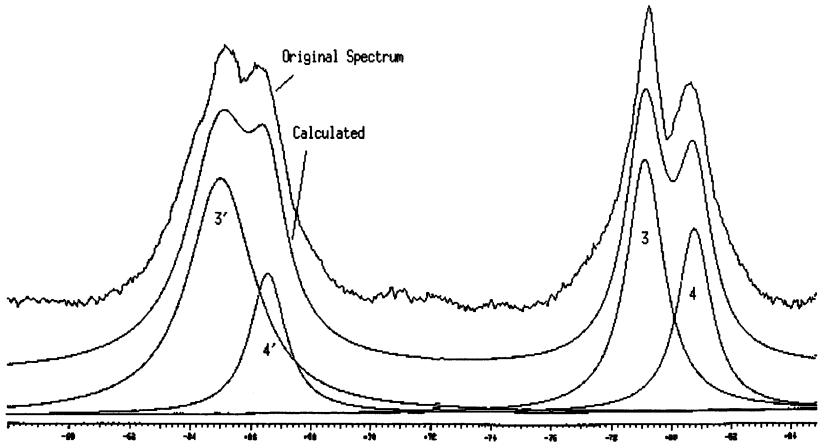

Figure 9. Deconvolution of the ^{29}Si NMR spectrum of fraction 5.

Table 6. Mole Fraction of Structural Units by ^{29}Si NMR Deconvolution

	$T^{Me}M$ (**3′**)	T^{Me} (**4′**)	$T^{Ph}M$ (**3**)	T^{Ph} (**4**)	total 3+3′	T_2(OZ)	M total	M′on T_3	Δ(3+3′-M′)
fraction 4	0.270	0.092	0.183	0.096	0.453	0.040	0.319	0.303	0.150
fraction 5	0.272	0.116	0.185	0.122	0.457	0.029	0.277	0.275	0.182
fraction 6	0.231	0.157	0.134	0.182	0.365	0.027	0.268	0.261	0.104
fraction 13	0.183	0.238	0.131	0.215	0.314	0.033	0.198	0.192	0.122

was 2:3 based entirely on statistical considerations. Consequently, the total amount of M^{Vi} connected to T_3 silicon was estimated by subtracting the amount of M^{Vi} connected to T_2 silicon, and the results are compared with the total content of **3** and **3′** in Table 6. Interestingly, the total content of **3** and **3′** was significantly higher (0.10−0.18 mol) than the M content determined from the analysis of the ^{1}H or ^{29}Si NMR spectra. These results suggested that the resonances assigned to **3** or **3′** possibly contain contributions from $T^{Ph}(T^R)_3$ (**4**) or $T^{Me}(T^R)_3$ (**4′**) silicons constrained in multiring or cage structures since resonance from this T group tended to shift further downfield.[46] The results also showed that the $T^{Me}T^R{}_3$ (**4′**) content was lower than that of $T^{Ph}T^R{}_3$ (**4**). Considering a T^{Me}/T^{Ph} ratio of greater than 1 for the individual fractions, it is plausible that either more T^{Me} is associated with M^{Vi} groups or more T^{Me} is involved in a constrained multiring or cage environment, possibly due to smaller size of the methyl group relative to the phenyl group.

FTIR Analysis. Infrared spectroscopy has been used as a valuable tool to analyze resin bonding and structures in siloxane materials.[48] The characteristic asymmetric absorption of SiOSi groups in the 1030−1150 cm^{-1} region was found to be dependent upon the length of the repeating units, the size of the siloxane rings, and the symmetry of the molecules (cage vs ladder).[49−53] For example, Brown[51] reported in a previous publication that the interconversion between cage and ladder phenylsilsesquioxanes can be monitored using infrared spectroscopy. The cage structure exhibited one absorption at 1120−1130 cm^{-1} (T_8, T_{10}, and T_{12}), while two absorptions at 1045 and 1135−1150 cm^{-1} were found for the proposed "ladder" polymer, regardless of the nature of the R group.

The IR spectra of fractions 1, 2, 3, and 13 (Figure 10) exhibited differences with respect to the asymmetric absorption of SiOSi groups in the 1030−1150 cm^{-1} region. As shown in Figure 9a, the spectrum for fraction 1 contained one strong peak at 1035 cm^{-1} and a

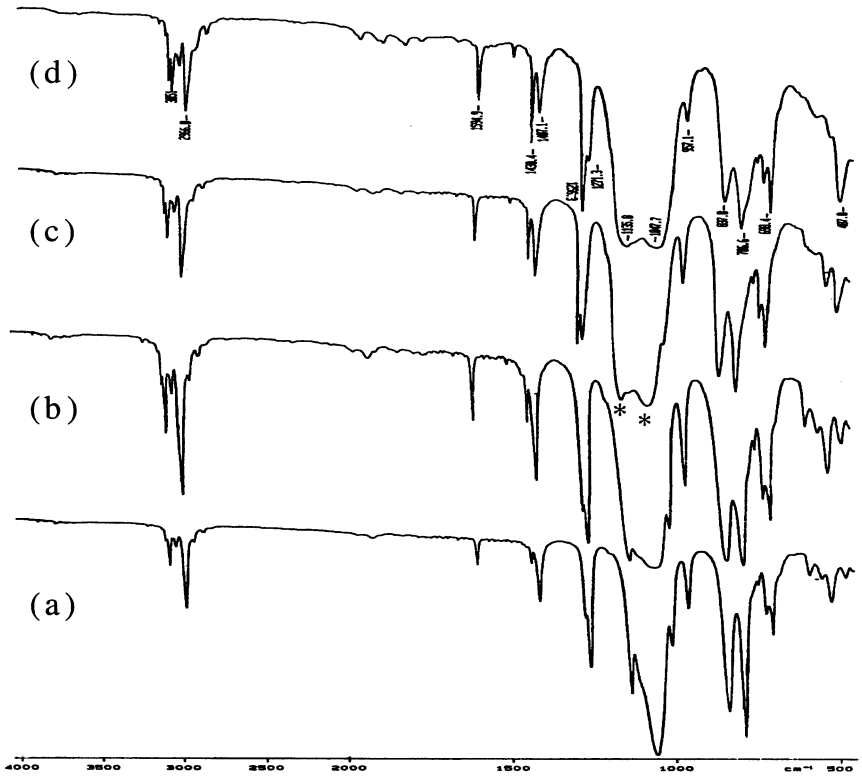

Figure 10. FTIR spectrum of (a) fraction 1, (b) fraction 2, (c) fraction 3, and (d) fraction 13.

shoulder at higher frequency attributed to asymmetric SiOSi stretching. The absorption intensity at 1135 cm^{-1} increased from fraction 1 to fraction 13. The IR spectra for fractions 4−13 are similar; therefore, only the data for fraction 13 are displayed in Figure 10d. The presence of only one strong absorption band at 1035 cm^{-1} for fraction 1 was consistent with the NMR and GC-MS results, indicating that the majority of species in the initial fractions were monomers or oligomeric species with very short SiOSi chains (e.g., TM_3 and T_2M_4).

SEC Analysis. The integration of on-line viscosity and light scattering (LS) detectors with the requisite concentration detector in size exclusion chromatography (SEC) enables the high-precision determination of polymer molecular weight, intrinsic viscosity, and molecular size distributions in a single experiment. The absolute molecular weight information from the light scattering (LS) detector is combined with the intrinsic viscosity (IV) data to determine the polymer molecular size, often expressed in terms of the polymer radius of gyration (R_g). This combination provided the capability of determining molecular weight and R_g at every elution slice across the entire SEC elution curve of the crude resin. From these results, the molecular weight dependence of polymer IV and R_g can be used to determine the differences in polymer branching and conformation between fractions. The SEC approach using multiple detectors permits direct resin conformation and branching determination, especially suitable for silsesquioxane resin characterization.

The absolute molecular weight and other important size and conformational information on the crude resin and fractions are summarized in Table 7. Initial experiments using toluene as the eluting solvent found that the light scatting signal was very weak even for the high-molar-mass fractions due to the similar refractive index of the resin and eluting solvent. However, the signal obtained in THF solution was strong and allowed

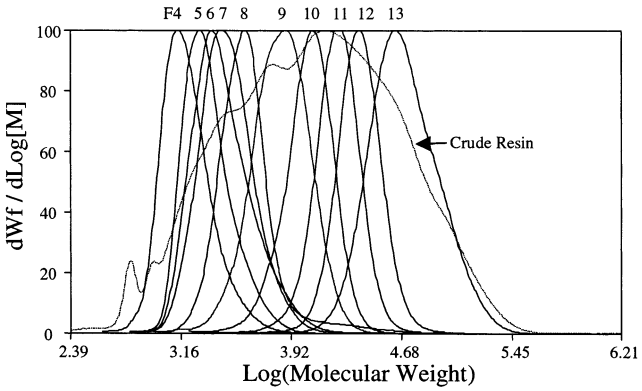

Figure 11. Overlaid SEC molecular weight distributions of the crude resin and fractions 4−13.

for accurate determination of the refractive index increment (d*n*/d*c*); hence, molecular weights for fraction 3 and above were determined. Figure 11 displays molecular weight distributions of fractions 4−13 along with the crude resin. The molecular weights of the first three fractions could not be accurately determined by light scattering technique due to weak instrument response.

The molecular weight of the crude resin material was determined to be 27 400 g/mol by light scattering, nearly 3 times greater than the 9800 g/mol^{-1} value determined by using SEC columns calibrated with polystyrene standards (PS). The molecular weight distributions for fractions 6−9 determined by MALDI−TOF MS are included in Table 8 by comparison to the values obtained by SEC techniques. For fractions 6−8, the values of M_n by MALDI−TOF MS are between those by SEC with PS and with triple detection. M_n values obtained for fractions 9 and 12 by SEC with the triple detection technique agreed reasonably well with MALDI data while SEC based on PS clearly underestimated the molar masses of these fractions.

Table 7. Molecular Weight Information by SEC with Triple Detection[a]

sample	M_w	M_n	M_z	M_w/M_n	R_{gw} (nm)	M−H *a*	d*n*/d*c*	IV_w (dL/g)
crude resin	27400	4930	103100	5.558	2.90	0.35	0.078	0.0388
F13	60800	44600	88900	1.363	4.95	0.50	0.083	0.0614
F12	26900	23300	31800	1.155	3.50	0.71	0.083	0.0469
F11	18800	16200	22100	1.16	2.96	0.72	0.083	0.0405
F10	12000	10200	14100	1.176	2.41	0.72	0.083	0.0341
F9	8060	6420	10200	1.255	2.00	0.61	0.083	0.0297
F8	7420	3780	83900	1.963	1.68	0.75	0.082	0.0261
F7	3460	2770	5030	1.249	1.41	0.65	0.082	0.0242
F6	3290	2530	5050	1.30	1.35	0.63	0.081	0.0227
F5	2480	2070	3290	1.21	1.21	0.70	0.079	0.0210
F4	1750	1440	2320	1.215	1.05	0.65	0.076	0.0197
F3	1450	990	1980	1.465	0.93	0.37	0.066	0.0171

[a] M_w = weight-average molecular weight; M_n = number-average molecular weight; M_z = *Z*-average molecular weight; Pd = polydispersity; R_{gw} = the weight-average radius of gyration; M−H *a* = the Mark Houwink "*a*" parameter; d*n*/d*c* = the refractive index increment; IV_w = the weight-average intrinsic viscosity.

Table 8. Molecular Weight (M_n) Determined by MALDI−TOF MS and SEC

fraction	MALDI M_n	MALDI M_w	SEC[a] M_n	SEC[a] M_w	SEC[b] M_n	SEC[b] M_w
6	1991	2264	1654	1904	2530	3290
7	2363	2934	2047	2396	2770	3460
8	3216	4084	2349	2759	3780	7420
9	7289	9243	4392	5356	6420	8060
12	25297	30370	11790	13451	23300	26900

[a] With polystyrene narrow standards. [b] With triple detection.

Because of the compositional differences among the resin fractions, the refractive index increment, d*n*/d*c*, was determined for each sample in the light scattering experiments. The data in Table 7 show that d*n*/d*c* increased from the low to the high molecular weight fractions and became constant after fraction 8 and is consistent with the polymer composition determined by NMR analysis. The value of M_w for fraction 8 was 7400 g/mol, and it represented a critical molecular weight above which relatively constant physical properties can be obtained. The R_{gw} ranged from 0.93 nm (M_w = 1450 g/mol) to 4.95 nm (M_w = 60 800 g/mol). The increase in R_{gw} was consistent with the intrinsic viscosity changes observed to occur from low to high molecular weight fractions.

Information on conformation of polymers can often be obtained from the Mark−Houwink plot (M−H plot) of log(IV) vs log(MW). The slope of this plot is referred as the M−H "*a*" parameter, which can be used to provide information on the relative conformations between the various fractions. The crude resin provided a M−H "*a*" parameter of 0.35, which is indicative of an average density structure with a "loose spherical" type of average conformation. The "*a*" parameter for fraction 3 was 0.37, while the "*a*" value reaches 0.61−0.72 for fractions 4−12, suggesting a random coil conformation for the molecules between M_w 1750 and 27 000 g/mol. The highest molecular weight fraction, fraction 13, has a relatively low "*a*" value of 0.50, suggesting a slightly different average conformation compared to fractions 4−12. The variation of "*a*" across the molecular weight distribution is believed to account for the low "*a*" observed for the crude resin.

The Mark−Houwink "*a*" parameter for a number of poly(phenylsilsesquioxane)s have been determined and used as supporting evidence for the proposed silsesquioxane structure.[3] The "*a*" values observed in poly(phenylsilsesquioxane)s typically range from 0.54 to 1.10 depending upon the synthetic conditions and the molecular weights of the materials.[54−59] Brown et al. proposed a linear, nearly rigid-rod double-chain structure for a poly(phenylsilsesquioxane) based on its high Mark−Houwink parameter (*a*: 0.92).[24] The lower "*a*" values in some high-molecular-weight polymers were attributed to branching in the high-molecular-weight materials. A wormlike chain model has been suggested for phenyl resins by Helminiak[60] and Shi et al.[61] The proposed fused-ring structure in this paper appears to be consistent with the molecular weight analysis, which exhibited flexibility to allow formation of random coil conformations at high molecular weight.

The degree of branching and cross-linking in the fractions can be evaluated by comparing the chromatograms obtained from refractive index, viscometry, and light scattering detectors. The light scattering experiment was especially sensitive to the high-molecular-weight materials. Fractions 4−7 and 9−12 all displayed excellent superimposed detector signals, and that for fraction 12 is shown in Figure 12a as an example. Because signals from light scattering and viscosity detectors are proportional to mass and concentration, while the refractive index signal is only concentration dependent, a slight shift of signal is observed in Figure 12a. The signal from the light scattering detector for fraction 8 (Figure 12b) revealed a shoulder at lower retention volumes, suggesting the presence of higher molecular weight species. The signals from fraction 13 (Figure 12c) showed the largest discrepancy, indicative of somewhat different structures. Combined with more compact conformation as evidenced by a lower M−H "*a*" parameter, we propose that the components in fraction 13 have a higher degree of branching.

In summary, SEC analysis with triple detection provides not only molecular weight information but also conformational and structural information for the resin fractions. The "*a*" parameter of the fractions indicated a variation of conformation across the molecular weight distribution. The random coil conformation established for the medium molar-mass fractions was consistent with fused-ring structures proposed by MS and NMR analysis. The highest molar-mass fraction very likely contained molecules with more branched structures.

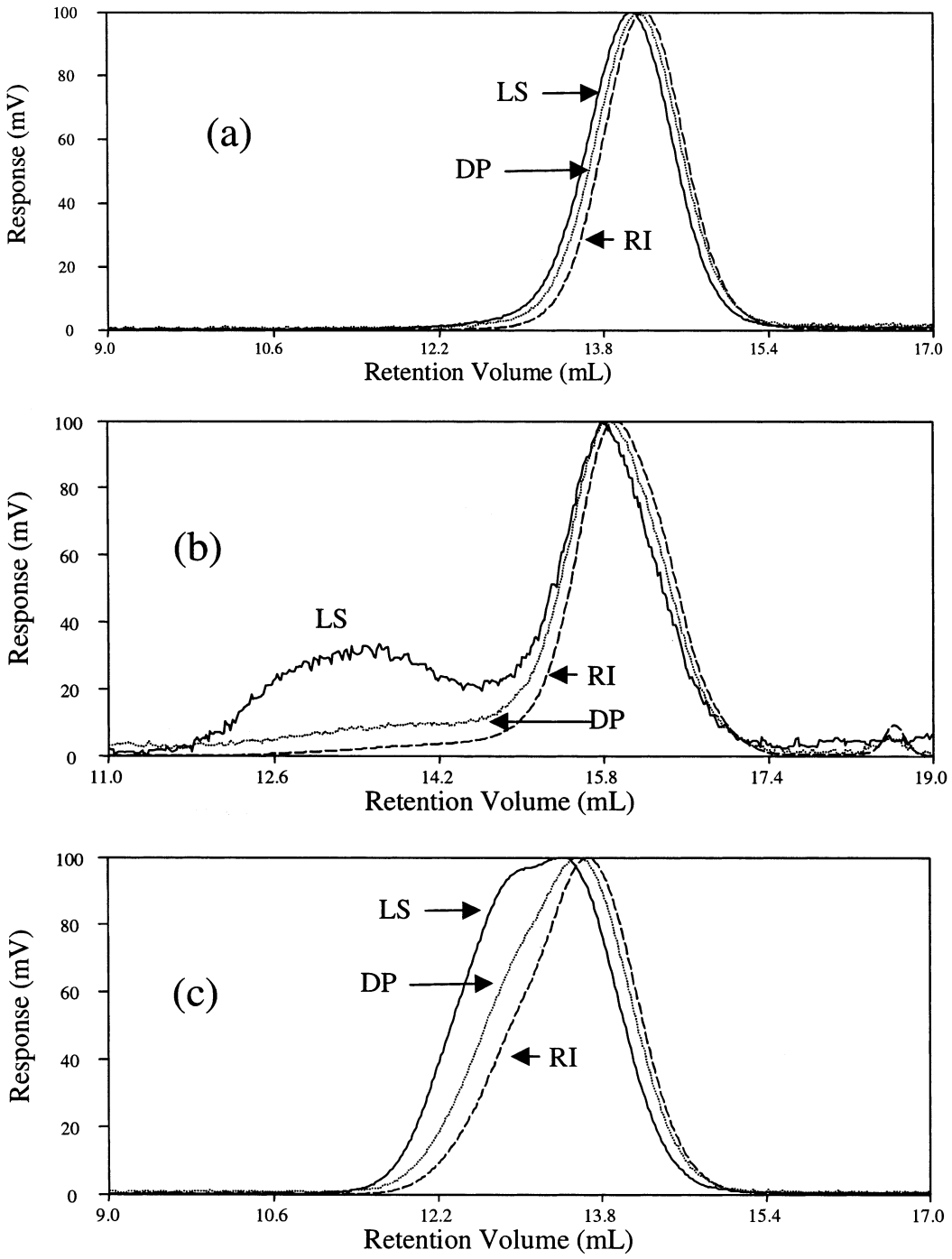

Figure 12. Overlay of detector signals for SEC: (a) fraction 12, (b) fraction 8, and (c) fraction 13.

Conclusions

On the basis of the compositional and structural analysis by MS, NMR, and FTIR, we propose that the $(PhSiO_{3/2})_{0.35}(MeSiO_{3/2})_{0.40}(Me_2ViSiO_{1/2})_{0.25}$ silsesquioxane adopts a structural feature containing fused siloxane rings via either adjacent (ladderlike) or nonadjacent vertexes (cagelike). Conformational analysis by SEC with triple detection supports a random coil conformation for intermediate molar-mass fractions, consistent with the proposed "linear" fused-ring structures. It should be pointed out that the model proposed in this paper only represents the main structural features of this resin, and it is highly possible that various types of structures coexist. We believe that the predominant structural features, along with molecular weight distribution, play a critical role in controlling the material properties, and further work is in progress to uncover composition−structure−property relationship for complex silsesquioxane resins.

Acknowledgment. The authors thank Sanlin Hu, Patti Rolley, Jerry Garner, and Craig Yeakle for their discussions and assistance in carrying out this work.

References and Notes

(1) Voronkov, M. G.; Lavrent'yev, V. L. In *Inorganic Ring Systems*; Boschke, F. L., Ed.; Springer: Berlin, 1982; Vol. 102, pp 199−236.

(2) Provatas, A.; Matisons, J. G. *Trends Polym. Sci.* **1997**, *5*, 327−332.

(3) Baney, R. H.; Itoh, M.; Sakakibara, A.; Suzuki, T. *Chem. Rev.* **1995**, *95*, 1409−1430.
(4) Zank, G. A. In *Silicon Containing Polymers*; Jones, R. G., Ando, W., Chojnowski, J., Eds.; Kluwer Academic Publishers: Dordrecht, The Netherlands, 2000; pp 697−726.
(5) Laine, R. M.; Babonneau, F. *Chem. Mater.* **1993**, *5*, 260−279.
(6) Seyferth, D. *Materials Chemistry-An Emerging Discipline*; Interrante, L. V., Caspar, L. A., Ellis, A. B., Eds.; Advances in Chemistry Series 145; American Chemical Society: Washington, DC, 1995; pp 131−160.
(7) Atwell, W. H. Polymeric route to silicon carbide and silicon nitride fibers. In *Silicon-Based Polymer Science*; American Chemical Society: Washington, DC, 1990; pp 594−606.
(8) Hurwitz, F. I.; Hyatt, L.; Gorecki, J. D'Amore, L. *Ceram. Eng. Sci. Proc.* **1987**, *8*, 732−743.
(9) Hurwitz, F. I.; Farmer, S. C.; Terepka, F. M.; Leonhardt, T. A. *J. Mater. Sci.* **1991**, *26*, 1247−1252.
(10) Eguchi, K.; Zank, G. A. *J. Sol-Gel Sci. Technol.* **1998**, *13*, 945−949.
(11) Remenar, J. F.; Hawker, C. J.; Hedrick, J. L.; Miller, R. D.; Yoon, D. Y.; Kim, S. M.; Trollsas, M. *Polym. Prepr.* **1998**, *39*, 631−632.
(12) Hedrick, J. L.; Miller, R. D.; Hawker, C. J.; Carter, K. R.; Volksen, W.; Yoon, D. Y.; Trollsas, M. *Adv. Mater.* **1998**, *10*, 1049−1053.
(13) Remenar, J. F.; Hawker, C. J.; Hedrick, J. L.; Kim, S. M.; Miller, R. D.; Nguyen, C.; Trollsas, M.; Yoon, D. Y. *Mater. Res. Soc. Symp. Proc.* **1998**, *511*, 69−74.
(14) Hedrick, J. L.; Hawker, C. J.; Trollsas, M.; Remenar, J.; Yoon, D. Y.; Miller, R. D. *Mater. Res. Soc. Symp. Proc.* **1998**, *519*, 65−75.
(15) Nguyen, C. V.; Carter, K. R.; Hawker, C. J.; Hedrick, J. L.; Jaffe, R. L.; Miller, R. D.; Remenar, J. F.; Rhee, H. W.; Rice, P. M.; Toney, M. F.; Trollsas, M.; Yoon, D. Y. *Chem. Mater.* **1999**, *11*, 3080−3085.
(16) Chua, C. T.; Sarkar, G.; Chooi, S. Y. M.; Chan, L. *J. Mater. Sci., Lett.* **1999**, *18*, 1437−1439.
(17) Kohl, P. A.; Padovani, A.; Wedlake, M.; Bhusari, D.; Ann, S.; Allen, B.; Shick, R.; Rhodes, L. *Mater. Res. Soc. Symp. Proc.* **1999**, *565*, 55−61.
(18) Kohl, A. T.; Mimna, R.; Shick, R.; Rhodes, L.; Wang, Z. L.; Kohl, P. A. *Electrochem. Solid-State Lett.* **1999**, *2*, 77−79.
(19) Mikoshiba, S.; Hayase, S. *J. Mater. Chem.* **1999**, *9*, 591−598.
(20) Watanabe, T.; Ooba, N.; Hayashida, S.; Kurihara, T.; Imamura, S. *J. Lightwave Technol.* **1998**, *16*, 1049−1055.
(21) Popall, M.; Dabek, A.; Robertsson, M. E.; Valizadeh, S.; Hagel, O. J.; Buestrich, R.; Nagel, R.; Cergel, L.; Lambert, D.; Schaub, M. *Mol. Cryst. Liq. Cryst.* **2000**, *354*, 123−142.
(22) Buestrich, R.; Kahlenberg, F.; Popall, M.; Dannberg, P.; Muller-Fiedler, R.; Rosch, O. *J. Sol.-Gel Sci. Technol.* **2001**, *20*, 181−186.
(23) Tadanaga, K.; Ellis, B.; Seddon, A. B. *J. Sol-Gel Sci. Technol.* **2000**, *19*, 687−690.
(24) Brown, J. F., Jr.; Vogt, L. H., Jr.; Katchman, A.; Eustance, J. W.; Kiser, K. M. *J. Am. Chem. Soc.* **1960**, *82*, 6194−6195.
(25) Brown, J. F., Jr. *J. Polym. Sci., Part C* **1963**, *1*, 83−97.
(26) Prado, L.; Radovanovic, E.; Pastore, H. O.; Yoshida, I. V. P.; Torriani, I. L. *J. Polym. Sci., Part A* **2000**, *38*, 1580−1589.
(27) Harold, J. H.; Su, K.; Katsoulis, D. E.; Suto, M.; Stucky, G. D. *Chem. Mater.* **2001**, *14*, 1174−1182.
(28) Lichtenhan, J. D. *Comments Inorg. Chem.* **1995**, *17*, 115−130.
(29) Lichtenhan, J. D. In *Polymeric Material Encyclopedia*; Salamone, J. C., Ed.; CRC Press: New York, 1996; Vol. 10, pp 7768−7778.
(30) Feher, F. J.; Budzichowski, T. A. *Polyhedron* **1995**, *14*, 3239−3253.
(31) Bujalski, D. R.; Chen, H.; Zank, G. A.; Su, K., submitted to *Macromolecules*.
(32) Fenn, J. B.; Mann, M.; Meng, C. K.; Wong, S. F.; Whitehouse, C. M. *Science* **1989,** *246*, 64−71.
(33) Kebarle, P.; Tang, L. *Anal. Chem.* **1993**, *65*, 972A−986A.
(34) Karas, M.; Bachmann, D.; Hillenkamp, F. *Anal. Chem.* **1985**, *57*, 2935−2939.
(35) Tanaka, K.; Waki, H.; Ido, Y.; Akita, S.; Yoshida, Y.; Yoshida, T. *Rapid Commun. Mass Spectrom.* **1988**, *2*, 151−153.
(36) Hillenkamp, F.; Karas, M.; Beavis, R. C.; Chait, B. T. *Anal. Chem.* **1991**, *63*, 1193A−1203A.
(37) Comisarow, M. B.; Marshall, A. G. *Chem. Phys. Lett.* **1974**, *25*, 282−283.
(38) Marshall, A. G.; Grosshans, P. B. *Anal. Chem.* **1991**, *63*, 215A−229A.
(39) Amster, I. J. *J. Mass Spectrom.* **1996**, *31*, 1325−1337.
(40) Marshall, A. G. *Acc. Chem. Res.* **1996**, *29*, 307−316.
(41) Tecklenburg, R. E.; Wallace, W. E.; Chen, H. *Rapid Commun. Mass Spectrom.* **2001**, *15*, 2176−2185.
(42) Analytical data for as-synthesized resin: $M_n = 1674$; $M_w = 2468$. ^{1}H NMR ($CDCl_3$, 200.1 MHz, ppm): 0.10 (CH_3), 3.50 ($SiOCH_3$), 5.80 ($CH{=}CH_2$), 6.10 ($CH{=}CH_2$). ^{29}Si{^{1}H} NMR ($CDCl_3$, 79.4 MHz, ppm): −1.8 ($Me_2ViSiO_{3/2}$), −71.5 (Ph(ZO)-$SiO_{2/2}$) −78.5 ($PhSiO_{3/2}$), −80.0 ($PhSiO_{3/2}$).
(43) Analytical data for as-synthesized resin: $M_n = 2497$; $M_w = 12\,484$. ^{1}H NMR ($CDCl_3$, 200.1 MHz, ppm): 0.25 (br, CH_3), 3.52 ($SiOCH_3$), 5.80 ($CH{=}CH_2$), 6.09 ($CH{=}CH_2$), 7.10 (C_6H_5), 7.81 (C_6H_5). ^{29}Si{^{1}H} NMR ($CDCl_3$, 79.4 MHz, ppm): −2.8 ($Me_2ViSiO_{3/2}$), 157.5 (Me(ZO)$SiO_{2/2}$), −65.8 ($MeSiO_{3/2}$), −66.5 ($MeSiO_{3/2}$).
(44) Analytical data for as-synthesized resin: ^{1}H NMR ($CDCl_3$, 200.1 MHz, ppm): 0.25 (br, CH_3), 3.50 ($SiOCH_3$), 5.84 ($CH{=}CH_2$), 6.09 ($CH{=}CH_2$), 7.10 (C_6H_5), 7.81 (C_6H_5). ^{29}Si{^{1}H} NMR ($CDCl_3$, 79.4 MHz, ppm): −2.0 ($Me_2ViSiO_{3/2}$), −57.5 (Me(ZO)$SiO_{2/2}$), −65.8 ($MeSiO_{3/2}$), −70.5 (Ph(ZO)$SiO_{2/2}$), −80.0 ($PhSiO_{3/2}$).
(45) For $MeSi(OSiMe_2Vi)_3$: ^{29}Si{^{1}H} NMR ($CDCl_3$, 79.4 MHz, ppm): −3.85 ($OSiMe_2Vi$), −64.0 ($MeSiO_{3/2}$). For $PhSi(OSiMe_2Vi)_3$: ^{29}Si{^{1}H} NMR ($CDCl_3$, 79.4 MHz, ppm): −2.20 ppm ($OSiMe_2Vi$), −77.8 ($PhSiO_{3/2}$).
(46) Williams, E. A. Recent Advances in Silicon-29 NMR Spectroscopy. In *Annual Reports on NMR Spectroscopy*; Webb, G. A., Ed.; Academic Press: London, 1983; Vol. 15.
(47) The compound was received from Olga Shchegolikhina, Russian Academy of Sciences.
(48) Lipp, E. D.; Smith, A. L. Infrared, Raman, Near-Infrerad, and Ultraviolet Spectroscopy. In *The Analytical Chemistry of Silicons*; Smith, A. L., Ed.; Wiley: New York, 1991.
(49) Brown, J. F., Jr.; Vogt, L. H., Jr.; Prescott, P. I. *J. Am. Chem. Soc.* **1964**, *86*, 1120−1125.
(50) Adachi, H.; Adachi, E.; Hayashi, O.; Okahashi, K. *Rep. Prog. Polym. Phys. Symp. Proc.* **1991**, *227*, 95.
(51) Takiguchi, T.; Fujikawa, E. Yamamoto, Y.; Ueda, M. *Nipon Kagaku Kaishi* **1974**, 108.
(52) Adachi, H.; Adachi, E.; Hayashi, O.; Okahashi, K. *Rep. Prog. Polym. Phys. Jpn.* **1986**, *29*, 257.
(53) Xie, Z.; He, Z.; Dai, D.; Zhang, R. *Chin. J. Polym. Sci.* **1989**, *7*, 183−188.
(54) Brown, J. F., Jr.; Vogt, L. H., Jr.; Katchman, A.; Eustance, J. W.; Kiser, K. M.; Krantz, K. W. *J. Am. Chem. Soc.* **1960**, *82*, 6194−6195.
(55) Helminiak, T. E.; Gibbs, W. E.; Benner, C. L. *Polym. Prepr.* **1967**, *8*, 284−291.
(56) Tsvetkov, V. N.; Andrianov, K. A.; Okhrimenko, G. I.; Vitovskaya, M. G.; Rjumtsev, E. I.; Shtennikova, I. N. *Eur. Polym. J.* **1971**, *7*, 1215−1230.
(57) Tsvetkov, V. N.; Andrianov, K. A.; Makarova, N. N.; Vitovskaya, M. G.; Rjumtsev, E. I.; Shtennikova, I. N. *Eur. Polym. J.* **1973**, *9*, 27−34.
(58) Andrianov, K. A.; Zhdanov, A. A.; Levin, V. Y. *Annu. Rev. Mater. Sci.* **1978**, *8*, 313−326.
(59) Kovar, J.; Mrkvickova-Vaculova, L.; Bohdanecky, M. *Makromol. Chem.* **1975**, *176*, 1829.
(60) Helminiak, T. E.; Berry, G. C. *J. Polym. Sci., Polym. Sci. Polym. Symp.* **1978**, *65*, 107−123.
(61) Shi, L.; Zhang, X.; Si, Y.; Ye.; M.; Li, D. *Chin. J. Polym. Sci.* **1987**, *5*, 359.

MA025652H